SMA Newsletter

Submillimeter Array Newsletter | Number 23 | January 2017

CONTENTS

FROM THE DIRECTOR

Dear SMA Newsletter readers,

The SMA has undergone a rapid increase in spectral throughput this past year as a result of the full implementation of the SWARM correlator. In dual-receiver operation, SWARM now accommodates the full 8 GHz double-sideband bandwidth, from each of two receivers. After sideband separation in processing, this translates into 16 GHz dual-polarized sky coverage with both receivers tuned identically, or 32 GHz sky coverage with offset tuning. A sample spectrum recently taken towards Orion, with the 230 and 240 GHz receivers tuned to deliver continuous frequency coverage from 213 to 245 GHz, is reproduced on page 15 of this Newsletter. The original SMA ASIC correlator has been decommissioned and we plan to offer full SWARM operation as standard for upcoming semester, 2017A.

Supported by ongoing improvements in receiver sensitivity and bandwidth, the successful deployment of SWARM, and the ASIAA-sponsored workshop 'SMA Science in the Next Decade', I am happy to report that the SMA Governing Board recently endorsed a three-year upgrade plan which we are calling the wSMA. The wSMA will offer even wider bandwidth operation than the current SMA, with improved sensitivity. Refer to page 17: Introducing the wSMA – A Major Upgrade to the SMA Receiver Systems for details . Once implemented, these plans will enable the SMA to continue to produce the highest quality science through the next decade.

Best wishes for 2017.

Ray Blundell

A KEPLERIAN DISC AROUND A MASSIVE YOUNG PROTO-O STAR

John D. Ilee (IoA, Cambridge), Claudia J. Cyganowski (St Andrews), Pooneh Nazari (St Andrews), Todd R. Hunter (NRAO), Crystal L. Brogan (NRAO), Duncan H. Forgan (St Andrews) and Qizhou Zhang (CfA)

The process of low-mass star formation is relatively well understood, due to the large number and proximity of such young objects to Earth. In contrast, the processes that govern the formation of massive stars (M > 8–10 M⊙) are not well characterised (see Beltran & de Wit 2016 for a review). There are many factors that contribute to the extreme difficulty in observing young, massive stars directly. Short formation timescales (10^4 — 10^5 yrs, Davies et al. 2011) mean there are few examples of these objects located close to Earth, and also that they spend their formative years entirely embedded. Issues such as these mean that, in particular, it is not yet clear whether circumstellar accretion discs surround massive young stellar objects (MYSOs) of all masses and evolutionary stages. Convincing candidates for Keplerian discs around embedded O-type protostars are proving to be particularly elusive. However, recent studies have yielded a handful of candidates (Jimenez-Serra et al. 2012, Wang et al. 2012, Hunter et al. 2014, Johnston et al. 2015, Zapata et al. 2015, Chen et al. 2016). Thus, in order to determine whether massive stars form in a similar way to their lower mass counterparts, we must perform high resolution observations and modelling of the gas and dust surrounding individual high-mass protostars.

G11.92-0.61 MM1 is one of three compact millimetre continuum cores detected within an infrared dark cloud (IRDC) around the region (Cyganowski et al. 2011, see **Figure 1, left**). In this work, we use the SMA and VLA to study the dust and molecular gas kinematics toward MM1 (Ilee et al. 2016). For the SMA, we used the very-extended configuration at 1.3mm to reach a 0.4" beam. We detect velocity gradients in several molecular lines — CH_3OH, C_2H_5CN, OCS, HNCO, H_2CO, DCN and CH_3CN. The first moment maps of the emission of the CH_3CN k=3 transition are displayed in **Figure 1 (right)**. Many different chemical species and transitions ranging in excitation energy share remarkably consistent velocity gradients, the position angle of which is ~90 degrees to that of the large scale bipolar outflow, and several lines show evidence of infall motions.

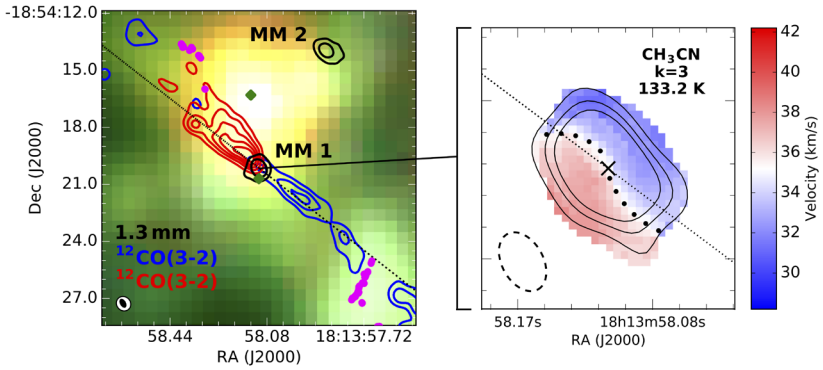

Figure 1: Left: Contours of SMA 1.3mm continuum (black, very-extended configuration) and blue/redshifted $^{12}CO(3–2)$ emission (extended configuration) overlaid on a three-colour Spitzer image (RGB: 8.0, 4.5, 3.6μm) clearly showing the well collimated outflow originating from MM1. Magenta symbols are Class I CH_3OH masers tracing outflow shocks, and green symbols are Class II masers tracing massive protostars. **Right:** First moment map of the CH_3CN k = 3 transition toward MM1, showing rotation about the outflow axis. The large black dots indicate the twisted structure in the zero-velocity gas, opposing the direction of outflowing material, indicative of infall towards the central object.

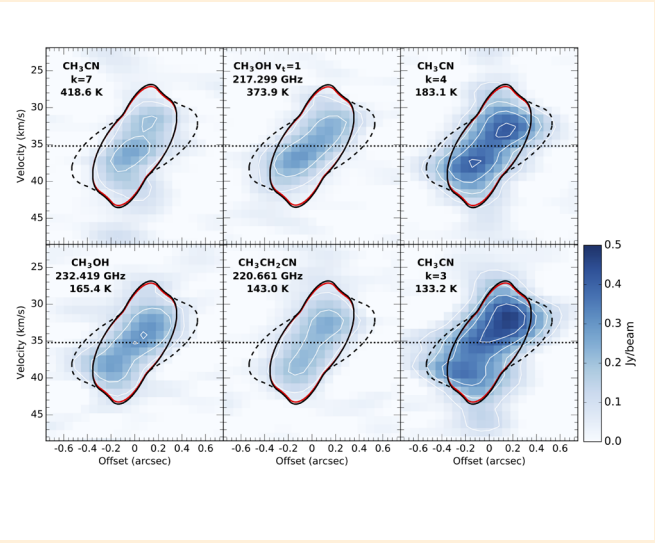

Figure 2: Position-velocity diagrams of selected lines toward MM1, ordered by decreasing E_{upper}. The systemic velocity of the system, 35.2 km s^{-1}, is shown with a dotted line. Overlaid are best fitting models from the centroid analysis. The best fit model for all lines, excluding CH_3OH (M_{enc} = 60M⊙, i = 35°, R_o = 1200au) is shown with a solid black line, and the best fit model for CH_3OH lines only (M_{enc} = 34 M⊙, *i* = 52°, R_o = 1200 au) is shown with a solid red line. These two models are almost identical in position-velocity space. The dashed black line shows a model identical to that of the best fitting disc model for all lines (excluding CH_3OH), but with R_o = 1800au, providing a better fit to some transitions.

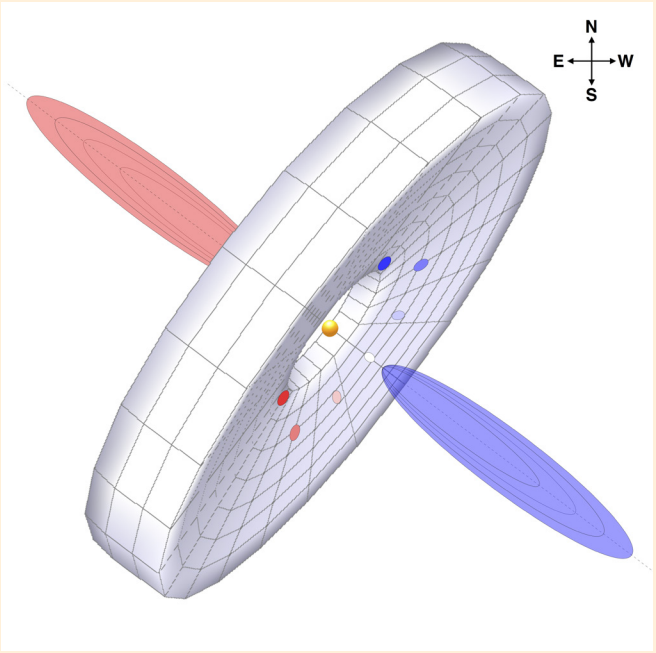

Figure 3: A proposed morphology for MM1. The maximum velocity gradient obtained from the line channel analysis (red-blue points) lies perpendicular to the axis of the molecular outflow. The closed loop structure of the channel centroids for many of the emission lines can be explained by a flared, optically thick Keplerian disc, viewed at an intermediate inclination. Such a disc would also exhibit a hot spot in temperature towards the South-West, as seen from our analysis of the CH_3CN gas properties.

For the compact lines, we calculate the spatial position of the centroid of emission for each channel. These centroids trace a looped structure, with the most red and blue shifted channels being closest together. We model the centroid positions of all lines using a geometrically thin Keplerian disc. We take the first moment of the model and compare with the centroid positions. Modelling of lines indicates a disc surrounding an enclosed mass of ~30—60M⊙, inclined at ~35—50 degrees, with an outer radius of ~1200 au. **Figure 2** shows the position-velocity diagram of several molecular lines, showing good agreement with the best fitting model from the centroid analysis.

To determine the physical properties of the gas around MM1, we modelled the line intensities and profiles of the CH_3CN and $CH_3{}^{13}CN$ emission line ladders. In order to adequately reproduce the spectra, we required two components of emitting material — a cooler (~150 K) and denser (~10^{18} cm^{-2}) component, along with a warmer (~230 K) and less dense (~10^{16} cm^{-2}) component. Spatial maps of gas properties show a hot spot in temperature towards the South-West of the continuum peak.

Modelling of the cm-mm wavelength SED toward MM1 suggests the presence of ionised gas which is best reproduced by a model including dust emission, a compact ionised jet (~17 au), and an unresolved hypercompact HII region (~20 au) — consistent with the scenario in which these regions are gravitationally 'trapped' by an accretion flow (e.g. Keto 2003, 2007).

In combination, our results suggest that G11.92–0.61 MM1 is likely a young proto-O star, in a swollen, non-ZAMS configuration, surrounded by a Keplerian disc with a morphology similar to that shown in **Figure 3**. Our observations and modelling support a self-consistent picture in which accretion is ongoing, and a high accretion rate governs many observable properties, including the presence of a gravitationally trapped hypercompact HII region and a moderate luminosity (~10^4 L⊙) for a massive (~30–60M⊙) central star.

Given the large disc-to-star mass ratio suggested by our observations, we also tested the propensity of the MM1 disc to be undergoing self-gravitating fragmentation (Forgan et al. 2016). We find that MM1 has a high chance of fragmenting, and may therefore have as-yet-unresolved low mass stellar companions. We will investigate this hypothesis with ALMA Cycle 4 observations in 2017.

REFERENCE

- Beltran M. T., de Wit W. J., 2016, A&ARv, 24, 6
- Chen H.-R. V., Keto E., Zhang Q., Sridharan T. K., Liu S.-Y., Su Y.-N., 2016, ApJ, 823, 125
- Cyganowski C. J., Brogan C. L., Hunter T. R., Churchwell E., Zhang Q., 2011a, ApJ, 729, 124
- Davies B., Hoare M. G., Lumsden S. L., Hosokawa T., Oudmaijer R. D., Urquhart J. S., Mottram J. C., Stead J., 2011, MNRAS, 416, 972
- Forgan D. H., Ilee J. D., Cyganowski C. J., Brogan C. L., Hunter T. R., 2016, MNRAS, 463, 957
- Hunter T. R., Brogan C. L., Cyganowski C. J., Young K. H., 2014, ApJ, 788, 187
- Ilee J. D., Cyganowski C. J., Nazari P., Hunter T. R., Brogan C. L., Forgan D. H., Zhang Q., 2016, MNRAS, 462, 4386
- Jimenez-Serra I., Zhang Q., Viti S., Martin-Pintado J., de Wit W.-J., 2012, ApJ, 753, 34
- Johnston K. G., et al., 2015, ApJ, 813, L19
- Keto E., 2003, ApJ, 599, 1196
- Keto E., 2007, ApJ, 666, 976
- Wang K.-S., van der Tak F. F. S., Hogerheijde M. R., 2012, A&A, 543, A22
- Zapata L. A., Palau A., Galvan-Madrid R., Rodriguez L. F., Garay G., Moran J. M., Franco-Hernandez R., 2015, MNRAS, 447, 1826.

A FIRST LOOK AT THE GIANT MOLECULAR CLOUD POPULATION IN SPIRAL GALAXY NGC 300

Christopher M. Faesi (CfA), Charles Lada (CfA), Jan Forbrich (Univ. of Vienna)

Giant Molecular Clouds (GMCs) are the coldest, densest regions within the interstellar medium, and are the birthplaces of stars. To understand how stars form, it is therefore important to investigate the physical properties of GMCs. Over the past several decades, this has been done extensively in the Milky Way, leading to a multitude of catalogs and a basic understanding of GMC characteristics (e.g., Heyer & Dame 2015). From these studies, GMCs appear to have typical sizes of 10-100 parsecs, masses of 10^4 – 10^6 solar masses, and highly supersonic velocity dispersions. Furthermore, observations have revealed canonical relationships amongst GMC physical properties: the velocity dispersion scales as the size to the one-half power, mass goes as size squared, and the virial mass is proportional to the mass as directly measured from, e.g., carbon monoxide (CO), extinction, or dust (Larson 1981). These scaling relations have important physical implications for GMCs, including that they are turbulent, gravitationally bound, and have an approximately constant mass surface density (e.g., Solomon et al. 1987; Heyer et al. 2009; Lombardi et al. 2010).

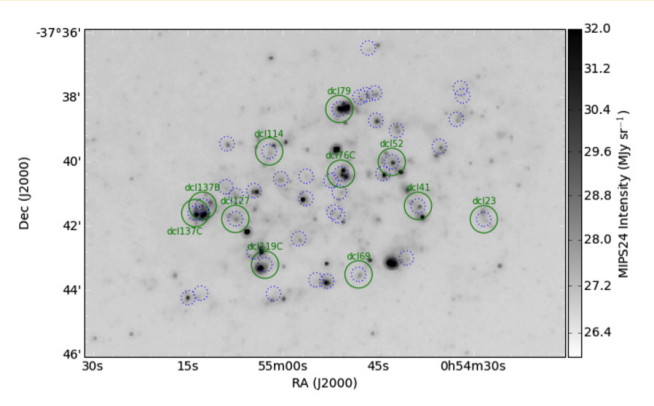

Figure 1: *Spitzer*/MIPS 24 μm image of NGC 300 with the positions observed with the SMA in CO(2-1) overlaid as green circles, with the circle sizes scaled to match the 51" SMA primary beam FWHM at 230 GHz. Blue dotted circles indicate the full sample of APEX CO detections.

While these so-called "Larson relations" appear to be robust within Milky Way disk GMCs, it has been challenging to assemble a comprehensive, uniform catalog of clouds due to our vantage point within the galaxy disk. In particular, distances toward Milky Way sources are notoriously difficult to measure, as sources appear projected in two dimensions on the sky and special techniques (and models) are needed to deproject them. This is a problem because several key physical properties rely on absolute distances, and so large measurement uncertainties on distance translate directly to large uncertainties on these properties. Furthermore, to understand GMCs as a broad population, it is necessary to study them in other galaxies and look for similarities and/or differences with Milky Way clouds. With the advent of millimeter interferometry, high-resolution CO observations have been extended to the nearest galaxies, including M31 (Rosolowsky 2007), M33 (Engargiola et al. 2003), and the LMC (Fukui et al. 2008), as well as more distant massive spirals such as M51 (Schinnerer et al. 2013). While the GMCs within the local group spiral galaxies (Milky Way, M31, M33) appear to fall mostly within the locus defined by the Larson size-linewidth (i.e., size-velocity dispersion) relation observed in the Milky Way, low metallicity and dwarf galaxies seem to deviate systematically below the trend (Bolatto et al. 2008), while GMCs in the massive spiral M51 show no clear evidence for a size-linewidth relation (Hughes et al. 2013).

To further investigate the nature of GMCs in a single, uniform sample in a low-metallicity spiral galaxy beyond the local group, we have conducted a survey of the nearby spiral galaxy NGC 300 using the Submillimeter Array (SMA). We targeted ten regions of active star formation in which we previously detected molecular gas (via its CO(2-1) emission; Faesi et al. 2014) with the single dish Atacama Pathfinder Experiment (APEX). **Figure 1** shows a *Spitzer*/MIPS 24um image of NGC 300 with the observed regions,

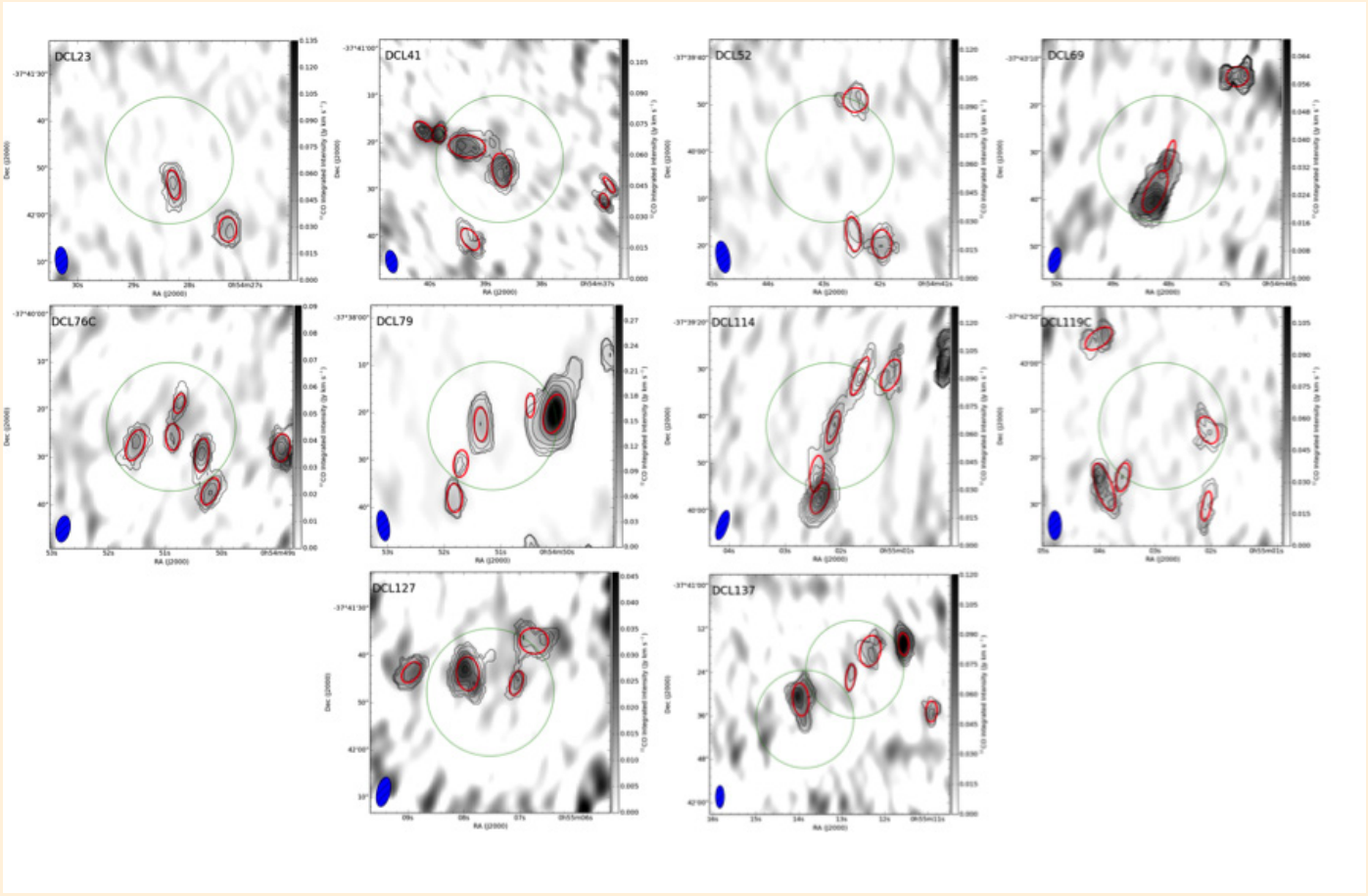

Figure 2: SMA CO(2-1) integrated intensity images of the ten regions observed in our campaign in which we resolve individual GMCs in NGC 300. Contours (in steps of multiples of the RMS noise) indicate the CPROPS-identified GMCs, with the red ellipses representing elliptical approximations for the cloud sizes and orientations. The background grayscale shows the full CO(2-1) data cube integrated over all GMC velocities. The green circles indicate the primary beam FWHM of 51". The synthesized beam is shown in the bottom left of each image.

which span a range of galactocentric radii and azimuth within the galaxy, overlaid.

Our observations resolve the single dish APEX detections into multiple GMCs in each region. **Figure 2** shows the SMA CO(2-1) integrated intensity images, in which we achieve a spatial resolution of approximately 4" (40 pc at the 1.9 Mpc distance of NGC 300). We utilized the CPROPS algorithm (Rosolowsky & Leroy 2006) to decompose the CO data cubes into discreet clouds and to characterize cloud properties. To convert measured CO emission into mass, we leverage the known metallicity gradient of NGC 300 to derive a radially dependent CO-to-H_2 conversion factor (Bolatto et al. 2013). Of the 45 clouds detected, 12 are spatially resolved and thus allow for robust characterization of GMC size. The SMA's wide bandwidth also allowed us to search for the CO isotopologues ^{13}CO and C^{18}O. We detect ^{13}CO in four clouds and find a median ^{12}CO/^{13}CO line flux ratio of 6.7, comparable to the value in the Milky Way (Solomon et al. 1979). We place a lower limit of 19 on the ^{12}CO/C^{18}O ratio.

We find that to the limit of our uncertainties, GMCs in NGC 300 appear to show a similar distribution, similar properties, and consistency with the same scaling relations as those observed in the Milky Way and M33 (**Figure 3;** Rosolowsky et al. 2003; Heyer et al. 2009). The GMC mass spectrum (i.e., the distribution of clouds by mass) has a slope of -1.80±0.07. We fit the size-linewidth relation using linear least squares fitting and find a power law slope of 0.52±0.20. The mass-size relation in NGC 300 is also qualitatively consistent with the Milky Way. The relation between virial mass and CO-derived mass also shows consistency. While the sample size is relatively modest and the measurement uncertainties large, these results suggest a level of universality in GMC properties within spiral galaxy disks in the local universe. Furthermore, the Milky Way, M33, and NGC 300 have different morphologies, sizes, and metallicities, demonstrating that these scaling relations may be independent of these parameters. Further high-resolution extragalactic studies are needed to test these conclusions in a larger sample of GMCs spanning the range of galaxy environments to better constrain the physics of star formation across the universe.

For more information, please refer to Faesi, C., Lada, C.J., & Forbrich, J. 2016, ApJ 821:125.

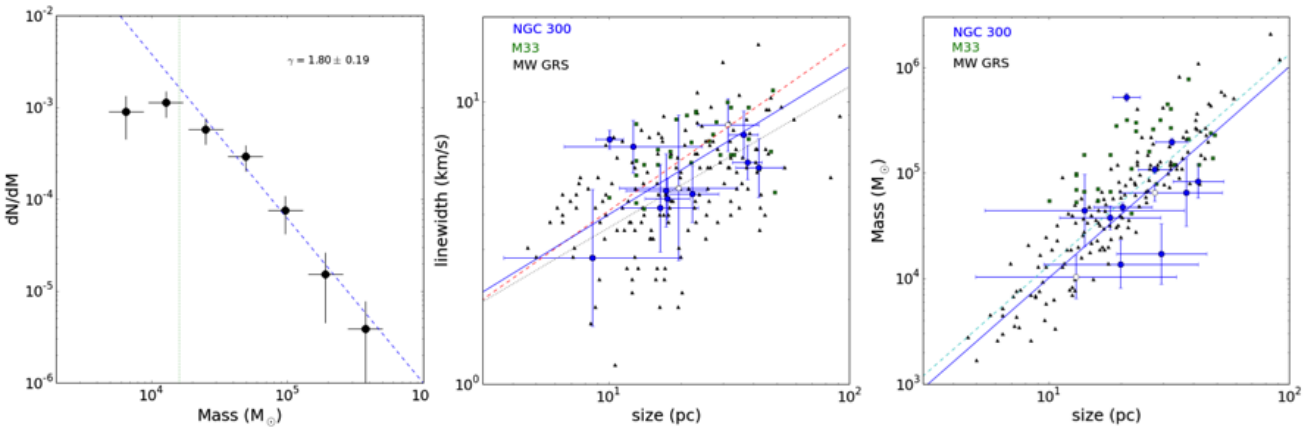

Figure 3 Left: GMC mass spectrum (left), size-linewidth relation (center), and mass-size relation (right) derived from our SMA CO(2-1) observations. The observed clouds from this work are shown as blue symbols and compared to GMCs in M33 from Rosolowsky et al. 2003 (green squares) and the Milky Way Galactic Ring Survey of Jackson et al. 2006 (black diamonds). Our results are consistent with those of other spiral galaxy disks.

REFERENCES

- Bolatto, A. D., Leroy, A. K., Roslowsky, E., Walter, F., & Blitz, L. 2008, ApJ, 686, 948
- Bolatto, A., Wolfire, M., Leroy, A. K. 2013, ARA&A, 51, 207
- Colombo, D., Hughes, A., Schinnerer, E., et al. 2014, ApJ, 784, 3
- Engargiola, G., Plambeck, R. L., Rosolowsky, E., & Blitz, L. 2003, ApJS, 149, 343
- Faesi, C. M., Lada, C. J., Forbrich, J., Menten, K. M., & Bouy, H. 2014, ApJ, 789, 81
- Fukui, Y., Kawamura, A., Minamidani, T., et al. 2008, ApJS, 178, 56
- Heyer, M., Krawczyk, C., Duval, J., & Jackson, J. M. 2009, ApJ, 699, 1092
- Heyer, M., & Dame, T. M. 2015, ARA&A, 53, 583
- Hughes, A., Meidt, S., Colombo, D., et al. 2013, ApJ, 779, 46
- Jackson, J. M., Rathborne, J. M., Shah, R. Y., et al. 2006, ApJS, 163, 145
- Larson, R. B. 1981, MNRAS, 194, 809
- Lombardi, M., Alves, J., & Lada, C. J. 2010, A&A, 519, L7
- Rosolowsky, E., Engargiola, G., Plambeck, R., & Blitz, L. 2003, ApJ, 599, 259
- Rosolowsky, E., & Leroy, A. 2006, PASP, 118, 590
- Rosolowsky, E. 2007, ApJ, 654, 240
- Schinnerer, E., Meidt, S., Pety, J., et al. 2013, ApJ, 779, 42
- Solomon, P. M., Sanders, D. B., & Scoville, N. Z. 1979, ApJL, 232, L89
- Solomon, P. M., Rivolo, A. R., Barrett, J., & Yahil, A. 1987, ApJ, 319, 730

SMA OBSERVATIONS OF THE EXTENDED ^{12}CO(J=6–5) EMISSION IN THE STARBURST GALAXY NGC 253

Melanie Krips (IRAM), Sergio Martin (ESO), Alison B. Peck (Gemini Observatory), Roberto Neri (IRAM), Mark Gurwell (CfA), Glenn Petitpas (CfA), Jun-Hui Zhao (CfA)

The 450 micron (690 GHz) atmospheric transmission window is difficult to use and possible at only a few sites worldwide, yet provides a unique view of warm and hot molecular gas and dust through CO line and submillimeter continuum emission. When coupled with high angular resolution (through interferometry), the analysis of spatially resolved warm molecular gas provides essential information for understanding the complexity of excitation conditions, chemistry and dynamics of molecular gas in various environments, including star-forming regions, active galactic nuclei and quiescent regions (e.g., Aladro et al. 2011; Krips et al. 2011, 2008; Martin et al. 2006).

We present interferometric observations of the extended ^{12}CO(J=6–5) line and 686GHz continuum emission in NGC253 carried out as a five point mosaic with the SMA at an angular resolution of ~4″ (Krips et al. 2016). NGC253 is one of the best studied nearby (~3.5Mpc, where 1″=17 pc; Rekola et al. 2005; Mouhcine et al. 2005) infrared bright starburst galaxies (3×10^{10} $L_{\odot}$; Telesco & Harper 1980). It is thus an ideal prototype to study the effects of a central starburst (=2-4$M_{\odot}$ yr^{-1} ; Minh et al. 2007; Ott et al. 2005; Bendo et al. 2015) on the dynamics, excitation conditions and chemistry of the surrounding molecular gas (e.g., Leroy et al. 2015; Meier et al. 2015; Bolatto et al. 2013; Sakamoto et al. 2011, 2006; Knudsen et al. 2007; Martin et al. 2006; Bradford et al. 2003). The molecular gas in the central kpc of NGC253 appears to be dominated by large-scale, low velocity shocks (e.g., Martin et al. 2006; Garcia-Burillo et al. 2000) as well as photodissociation regions (PDRs; Martin et al. 2009, Rosenberg et al. 2012 and 2014).

We compared our 690GHz data to three lower-J ^{12}CO transitions (J=1–0, J=2–1, J=3–2) and continuum emission at lower frequencies at similar angular resolution of ~4″ observed with ALMA and the SMA. Five of the eight ^{12}CO line peaks find counterparts in the mm and submm continuum emission underlying the thermal nature of the continuum emission from dust as suggested by the spectral index of 3 determined from the different frequencies (Figures 1&2). The continuum emission at the lowest frequency of 115GHz appears to exhibit already a significant contribution from non-thermal synchrotron and thermal free-free processes (between 15-80%) as supported by the spectral indices derived at cm wavelengths (Figure 1). We derive dust temperatures of ~10-25K for the different continuum peaks in the disk with low opacities of ~0.2 at 686GHz. However, we also find indications for a hotter dust component at least in the inner disk of NGC253 with dust temperatures exceeding 60K and at much larger opacities of around 4 at 686GHz. The latter dust component approaches the values found for ULIRGs such as Arp220. We estimate a total dust mass of a few 10^6 $M_{\odot}$ for the entire disk, splitting up into ~10^4-$10^5$$M_{\odot}$ for the GMCs at the individual continuum peaks. Based on the gas masses of each of the peaks, we find a gas-to-dust mass ratio of the order of ~100-1000.

The ^{12}CO(J=6–5) emission follows nicely the distribution of the molecular gas seen in the lower-J transitions with roughly eight peaks along the disk (Figure 2). Only few ^{12}CO(J=6–5) emission is detected close to the two shells emerging from the edges of the central disk. While the ^{12}CO line transition ratios do not vary significantly along the disk, the two shells show quite different ratios not only compared to the disk but also to each other (Figure 3). The line ratios found along the disk seem to necessitate a two-phase gas model in agreement with previous studies on NGC253 as well as multiple-^{12}CO observations on other active galaxies. This two-phase gas model is mainly based on two temperatures, a cool gas component at around T_{kin}=10K and hot gas component at around T_{kin}=300K. Following a similar argumentation to previous publications, the lower temperature gas is probably dominated by the PDR while the higher temperature gas is a consequence of the shocks found throughout the disk (see also Rosenberg et al. 2012, 2014). However, a possible contribution from cosmic rays,

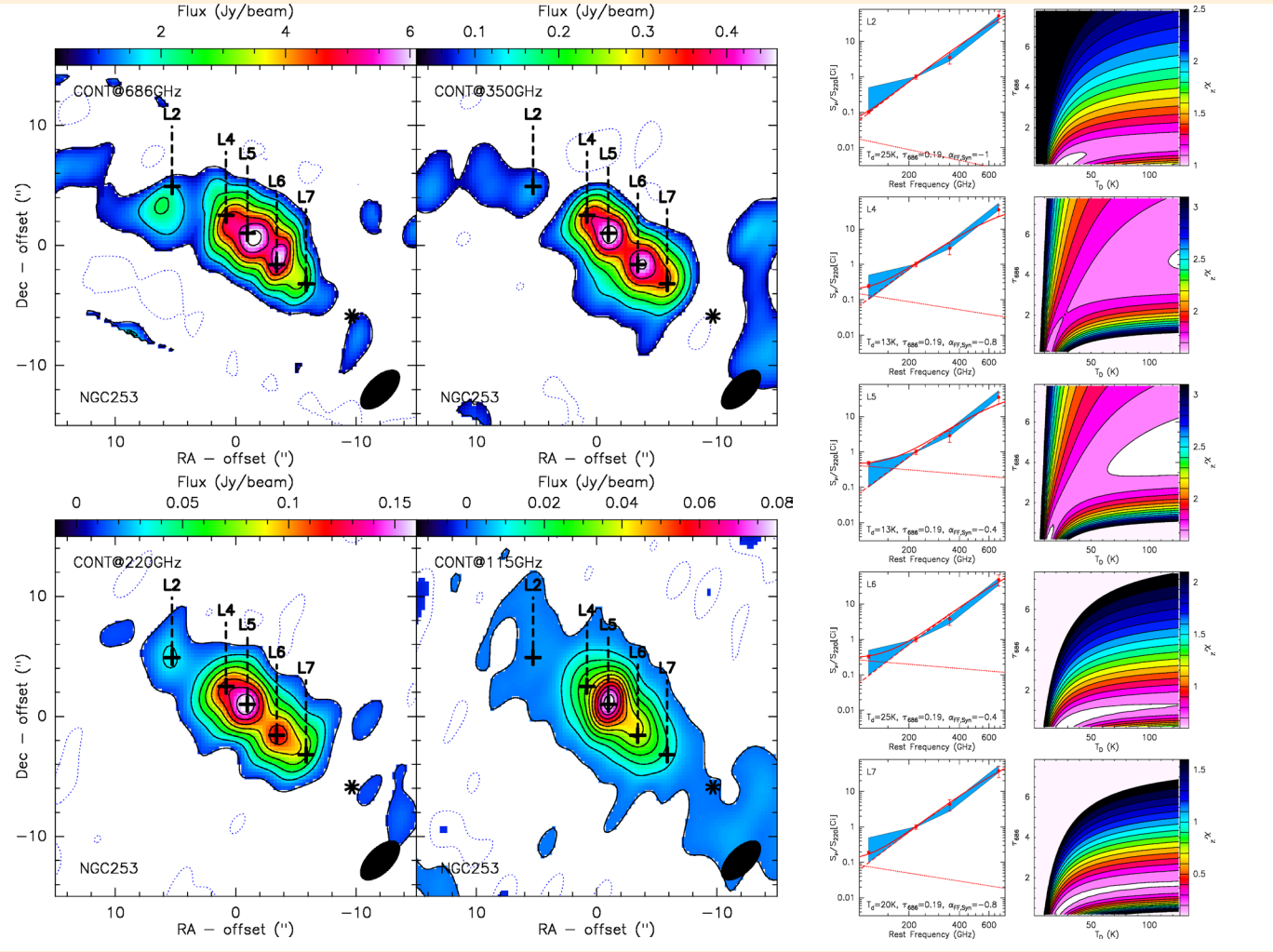

Figure 1: Continuum Emission in NGC253. *Left Panel:* Continuum emission at 686 GHz (panel 1, upper left), 350 GHz (panel 2, upper right), 220 GHz (panel 3, lower left) and 115 GHz (panel 4, lower right), all at a spatial resolution of ~4.2″ × 2.1″. The black crosses indicated in each panel mark the positions of the respective line emission peaks defined in Fig. 2 matching those of the continuum peaks shown here and being in good agreement with the 1.3 mm continuum emission peaks from Sakamoto et al. (2011). The black star marks the position of the western superbubble/shell from Sakamoto et al. (2006). Note, that the eastern superbubble/shell lies outside the maps and is not shown here since no continuum emission is detected around it. *Right Panel:* Continuum SED for the different continuum peaks (only peak fluxes taken for each frequency; left panel), normalised to the respective continuum fluxes at 230 GHz for each component and the corresponding best fit solution (i.e., lowest reduced χ^2 ; right panel) for each continuum peak assuming a dust emissivity of β =1.8. The dashed and dotted lines represent the thermal (from a modified black body) and non-thermal synchrotron plus thermal free-free contribution to the emission, while the solid line is the composite of both. The dashed line has been fitted to the data, while the dotted line was made using a fixed beta of 1.8 from Heesen et al. (2011). The blue shaded areas plotted in each panel on the left indicate the range of continuum fluxes found at the positions of L2-L7. T_d is the dust temperature , τ_{686} is the opacity at 686 GHz and $\alpha_{FF,Syn}$ is the spectral index coming from the free-free/synchrotron emission.

given the high cosmic ray ionisation rate within the disk, cannot be completely excluded for either temperature phase at this point although some simulations indicate only a minor role of cosmic ray heating (e.g., Rosenberg et al. 2014). While the eastern shell exhibits even warmer gas (T_{kin}>300K) with respect to the hot gas (T_{kin}≃300K) component of the disk, the western shell contains gas much cooler (T_{kin}≃60K) than the eastern shell but somewhere in between the two temperature gas components of the disk (T_{kin}^{cold} ≃10K and T_{kin}^{hot} ≃300K); the gas densities ($n(H_2)$ ≃5×10^3 cm^{-3}) and column densities (N(CO) ≃10^{18}cm^{-2}) are very similar between the two shells and the disk. This reflects either a different evolutionary stage of the shells, an additional, different or more efficient heating mechanism in the eastern shell, a very different nature of these two structures, or a combination thereof.

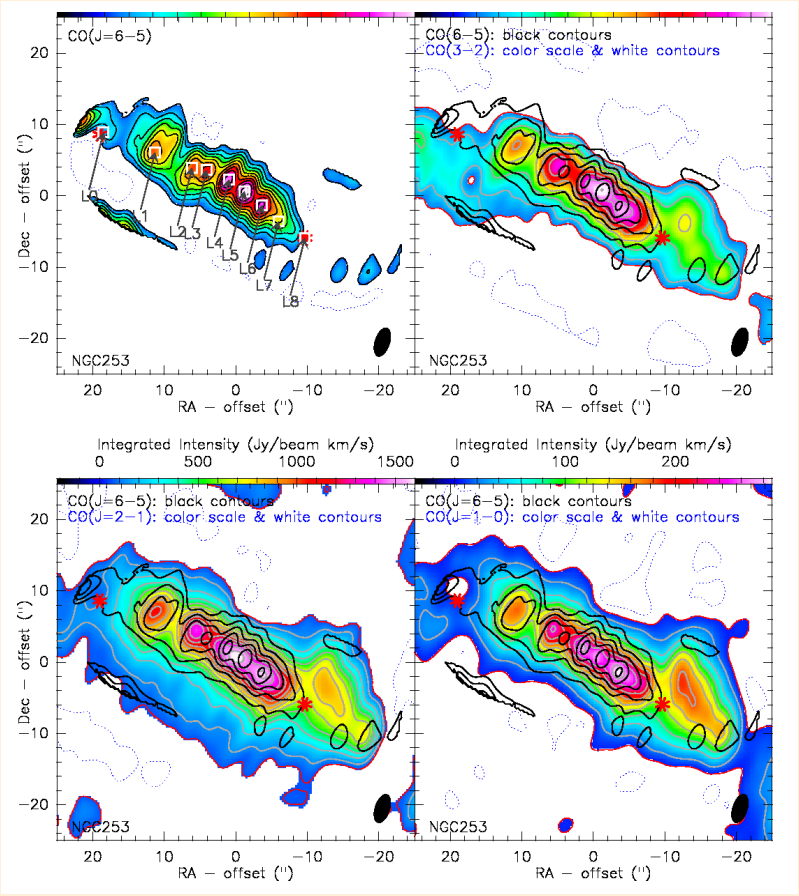

Figure 2: Panels comparing the flux distributions of the four ^{12}CO line transitions. Panel 1 (upper left) shows the ^{12}CO(J=6–5) emission in color scale and contours. Panel 2 (upper right) shows the ^{12}CO(J=3–2) emission (this paper and Sakamoto et al. (2011); in color scale and red and grey contours) overlaid with contours (in black) of the ^{12}CO(J=6–5) line emission. Panel 3 (lower left) shows the same but for the ^{12}CO(J=2–1) emission (taken from Sakamoto et al. 2011) overlaid with the contours of the ^{12}CO(J=6–5) emission. Panel 4 (lower right) shows the same but for the ^{12}CO(J=1–0) emission (taken from the ALMA science archive) overlaid with the contours of the ^{12}CO(J=6–5) emission. The red stars (inner and outer two white squares) mark the positions of the two shells (L0 and L8) from Sakamoto et al. (2006) and L1-L7 (white squares) with the corresponding arrows mark the line peaks of the ^{12}CO(J=6–5) emission in order to facilitate the discussion.

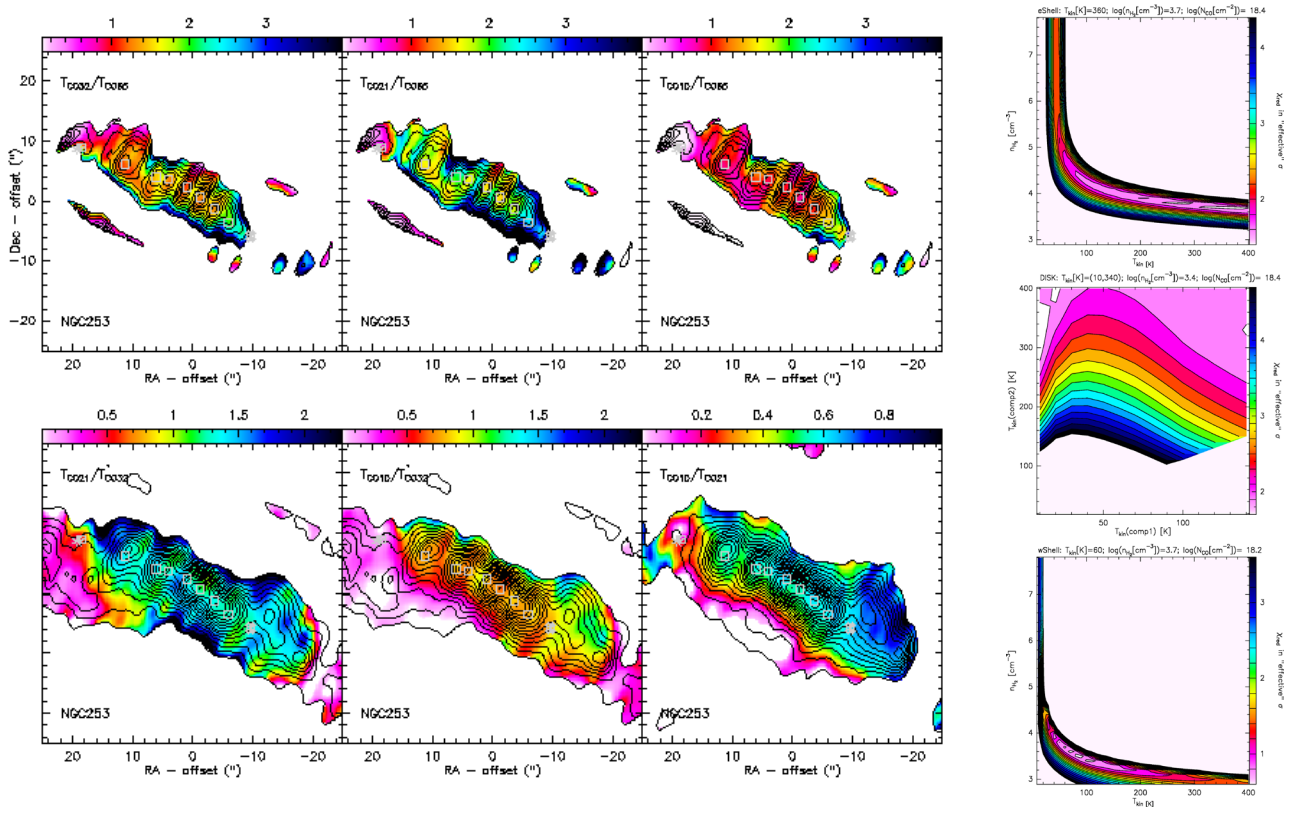

Figure 3: Temperature brightness ratios between the different integrated ^{12}CO line transitions. *Left Panel:* The grey symbols (squares and stars) are the same as in Fig. 2. Contours in the upper panels are those of the ^{12}CO(J=6–5) emission while those in the lower panels are from the ^{12}CO(J=1–0) line emission. *Right Panel:* Best fit solutions with the lowest χ^2red for the three different regions. For the one phase gas models of the western (wShell/L8) and eastern shells (eShell/L0; upper and lower panel) we plot the kinetic temperatures and CO column densities for a given H_2 density while for the two phase gas model we show the two kinetic temperatures for a given H_2 density and CO column density. The reduced χ^2_{red} can be seen as effective σs, meaning that a value of 1 (2,..) represents modelled line ratios that are on average within 1σ (2σ,..) of the respective observed line ratios. The solution with absolute lowest χ^2_{red} are given above each panel.

REFERENCES

- [1] Meier, D. S., Turner, J. L.; Beck, S. C. 2002, AJ, 124, 877
- [2] Turner, J. L., Beck, S. C., Benfold, D. J. & et al. 2015, Nature, 519, 331
- [3] Sakai, S., Ferrarese, L., Kennicutt, R. C., Jr., & Saha, A. 2004, AJ, 604, 42
- [4] Sargent, W. L. W., Searle, L. 1970, ApJL, 162, L155
- [5] van Zee, L., Skillman, E. D., & Salzer, J. J. 1998, AJ, 116, 1186
- [6] Kunth, D., Ostlin, G. 2000, A&AR, 10, 1
- [7] Beck, S. C., Turner, J. L., Ho, P. T. P. & et al. 1996, ApJ, 457, 610
- [8] Turner, J. L., Ho, P. T. P., & Beck, S. C. 1998, AJ, 116, 1212
- [9] Caldwell, N., & Phillips, M. M. 1989, ApJ, 338, 789
- [10] Calzetti, D., Meurer, G. R., Bohlin, R. C., et al. 1997, AJ, 114, 1834
- [11] Chandar, R. et al. 2005, ApJ, 628, 210
- [12] Harbeck, D., Gallagher, J., & GrnojeviĐ, D. 2012, MNRAS, 422, 629

A CANDIDATE HIGH REDSHIFT CLUSTER/ PROTOCLUSTER OF STAR-FORMING GALAXIES

D. L. Clements (ICL), F. Braglia (ICL), G. Petitpas (CfA), J. Greenslade (ICL) and the H-ATLAS Team

The early history of galaxy clusters is a poorly understood aspect of galaxy and large-scale structure formation. Hierarchical clustering models predict that massive elliptical galaxies will form in the cores of what will become the most massive galaxy clusters today, but the epoch of peak star formation for these galaxies is unclear. Large area surveys with the *Herschel Space Observatory* (Pilbratt *et al.* 2010), SCUBA2 (Dempsey *et al.* 2013), or the *Planck* all sky survey (*Planck* Collaboration 2011) are capable of finding candidates for study. Several such surveys have been undertaken combining *Planck* and *Herschel* data to identify candidate high redshift clusters while others have used *Herschel* data (*e.g.* Valtchanov *et al.* 2013; Dannerbauer *et al.* 2014; Rigby *et al.* 2014) or SCUBA2 data (Ma *et al.* 2015; Casey *et al.* 2015) alone or in combination (Noble *et al.* 2013). We report here on a project that uses the SMA to help confirm the existence of and determine the properties of high redshift cluster members around the lensed system HATLAS12-00 (Bussman *et al.* 2013).

HATLAS12-00 had already been identified as a candidate gravitationally lensed galaxy as a result of its high submm flux (i.e. F_{500}>100 mJy), red *Herschel* colors, and the lack of a bright optical or radio counterpart (see *e.g.* Negrello *et al.* 2010 for a discussion of the selection of lens candidates in H-ATLAS and other *Herschel* surveys). This source was therefore observed spectroscopically in the submm. A CO spectroscopic redshift of 3.26 was first suggested by Z-spec (Bradford *et al.* 2004) observations, then subsequently confirmed by observations by the CARMA interferometer (Leeuw *et al.* in prep) and the Zpectrometer instrument on the Greenbank Telescope (Harris *et al.* 2012). Additional followup observations in the optical, near-IR, submm and other wavelengths were targeted at the lensed z=3.26 source and the foreground objects responsible for the lensing, resulting in detailed analyses of this lensing system by Fu *et al.* (2012) and Bussmann *et al.* (2013). Their conclusions are that the z=3.26 source HATLAS12-00 is subject to gravitational lensing, with a magnification of 9.6 ± 0.5 in both the submm continuum and CO, and 16.7 ± 0.8 in the K' band, by two foreground galaxies, one at a spectroscopically determined redshift of 1.22, and another with photometry suggesting that it lies at a similar redshift. The

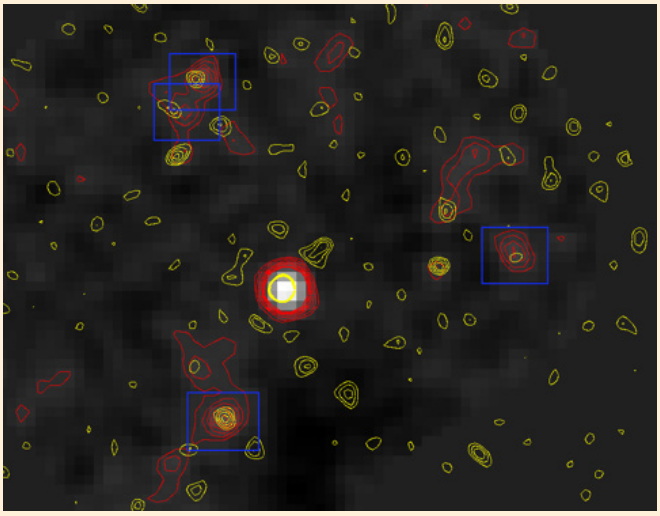

Figure 1: The LABOCA S/N image with red contours overlaid with the yellow SCUBA2 850 μm SNR contours. The central saturated source is the lensed galaxy HATLAS12-00 from Bussman *et al.* 2013. Contour levels for both LABOCA and SCUBA2 are set at 2,3,4... σ. A total of 17 other LABOCA and/or SCUBA2 sources are also found with S/N > 4σ in the surrounding field. Regions studied by the SMA are shown with the blue boxes, and contain the sources (from top to bottom) LABOCA_3, LABOCA_5, LABOCA_4, and LABOCA_2 (respectively).

submm photometry of HATLAS12-00 at 890 μm acquired with the Submillimeter Array (SMA) as part of this program (Fu *et al.* 2012; Bussmann *et al.* 2013) is fully consistent with the 870 μm and 850 μm fluxes derived for this source from the LABOCA and SCUBA2 data to be presented here. The spectral energy distribution (SED) of the lensed source, after correcting for the lensing amplification, is well matched by the optically thick SED model for Arp220 from Rangwala *et al.* (2011), with a lensing-corrected far-IR luminosity of 1.2 ± 0.2 x 10^{13} $L_{\odot}$, and an implied star formation rate of 1400 ± 300 $M_{\odot}$ yr^{-1}. In many ways the unlensed properties of this object match those of the broader population

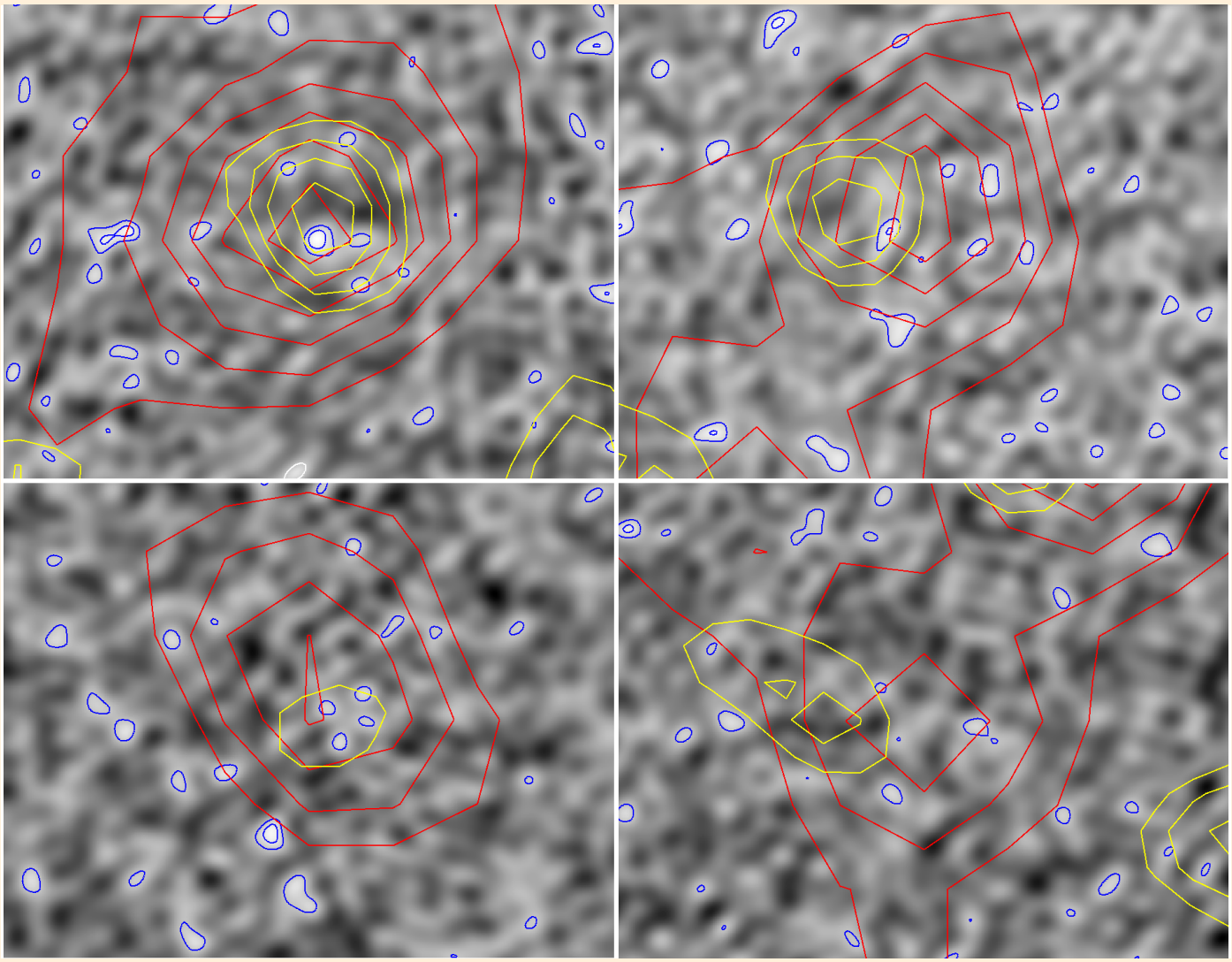

Figure 2: Mosaic of SMA observations (greyscale with blue contours) for sources detected in both SCUBA2 (yellow contours) and LABOCA (red contours) images. Clockwise from upper left the fields are LABOCA_2, LABOCA_3, LABOCA_4, and LABOCA_5. The contour levels for the SMA, LABOCA and SCUBA2 data are set at 2,3,4... σ. Each panel is 52" in height).

of bright submm selected galaxies first discovered by the SCUBA submm imager (see *e.g.* Chapman *et al.* 2005; Clements *et al.* 2008; Michalowski *et al.* 2010). The unlensed 870 μm flux of this object would be ~7.7mJy.

We observed a field of diameter ~600 arcsec around the position of the lensed source HATLAS12-00 with the LABOCA 870 μm imager on the APEX telescope (the Atacama Pathfinder EXperiment, Gusten *et al.* 2006), during ESO program 088.A-0929. APEX is a 12m diameter submm telescope situated in the Atacama Desert in Chile. Individual sources are extracted from the map using a source-finding algorithm which identifies peaks in a smoothed signal-to-noise map, produced by convolving the flux density map, weighted by the inverse of the variance, with the 18.6 arcsec full width half maximum (FWHM) beam. Peaks with a signal-to-noise ratio of at least 2.5 were selected as candidate sources, their flux (error) was then calculated as the value of the beam-convolved flux density (noise) map at the position of the peak. We detect seven peaks above a 4σ threshold, four of which have S/N > 5.

A field of diameter ~ 700 arcsec around the position of HATLAS12-00 was observed with the SCUBA2 850 & 450 μm imager (Holland *et al.* 2013) on the James Clerk Maxwell Telescope (JCMT) on Mauna Kea as part of a program to observe candidate clusters of dusty galaxies detected through cross matching *Planck* and *Herschel* sources. SCUBA2 provides an angular resolution of 14.5 arcsecs (FWHM) at 850 μm. Individual sources were extracted from the map by identifying peaks in the S/N map calculated by dividing the final beam convolved map by the noise map. Applying a 4-sigma threshold for detection, we find a total of 14 850 μm sources. Six of these, including the lensed source, have a S/N > 5.

Small regions around four of the sources detected by LABOCA and/or SCUBA2 were observed by the SMA for the purpose of confirming the existence of and determining the properties and position of the candidate cluster members to target for high-resolution follow-up observations. Four regions (see Figure 1) around HATLAS12-00 were observed at the SMA in Compact configuration on 2013 April 7 UTC and 2013 May 16 UTC. The SIS receivers were tuned to an LO frequency of 270.0 GHz. Both observations were made in good conditions, with $\tau_{225} \sim 0.07$ and 10-25% humidity. An additional track in SubCompact configuration was obtained on 2013 May 13 UTC in slightly worse conditions ($\tau_{225} \sim 0.07$ and only 6 antennas) but was combined with the other two tracks for a slight improvement in SNR and a final beam of about 2.7 x 2.3 arcsecs. The sources were observed using track sharing, with the array switching between each source throughout the track. 3C279, 3C273 and 1058+015 were used as gain calibrators for these observations, while MWC349a and Titan were used as flux calibrators. 3C279 and 2015+371 were used as bandpass calibrators. The data were calibrated in MIR and imaged with MIRIAD (Sault *et al.* 1995). The noise in the final coadded maps ranged from 1 to 1.3 mJy. A secure source was only detected in the map of LABOCA_2 with a flux of 4.2 ± 1 mJy. The other sources often show one or more 2+ σ detections, which could be candidate cluster member detections, but the signal to noise is not high enough in these data. The estimated fluxes and flux limits agree with the predicted 270 GHz fluxes of 8, 4, 6 and 4 mJy for LABOCA_2, LABOCA_3, LABOCA_4 and LABOCA_5 respectively.

Multiwavelength followup observations of the SMA identified LABOCA_2 show it is also detected by *Spitzer* at 3.6 and 4.5 μm, and in subsequent near-IR imaging using the VLT. Examination of SDSS images at the position of this source fails to find any optical counterpart, implying that the *i*-band magnitude of the source is fainter than the 21.3 magnitude *i*-band limit of SDSS. Deeper optical observations of this source obtained with white light (*i.e.* filterless) observations at the WHT also fail to find an optical counterpart. Photometric redshift analysis of the optical/NIR SED of this source indicates a redshift >2, potentially similar to that of HATLAS12-00 but not compatible with redshifts ~1.

Given the lack of secure SMA detections in these data, the existence of a cluster comes down to a statistical study using expected number counts of high-*z* targets compared to the field counts.

There is an overdensity of *Herschel* sources around HATLAS12-00 which has a probability of 5×10^{-4} of arising at random. While the overdensity is highly significant, the underlying field source counts are sufficiently high that it is unlikely that all of the sources around HATLAS12-00 are members of the overdensity. Analysis suggests that a significant fraction of the sources we have detected around HATLAS12-00 are likely to lie in an overdensity of objects. It is a natural step from this result to think that these objects are part of a single coherent physical structure, possibly a cluster or protocluster of galaxies.

Obtaining spectroscopic redshifts for the *Herschel* and submm sources we have uncovered is necessary for properly understanding this overdensity. Unfortunately such data are not yet available, but we can get some hints as to what might be going on by applying far-IR photometric redshift techniques, similar to those used by Noble *et al.* (2013) in studying a submm source overdensity at a suggested redshift of $z \sim 3$ which they uncovered behind the $z = 0.9$ supercluster RCS 231953+00. This process produces a similar result to that found by comparing the color tracks of template sources to the observed colors of our sources: the higher luminosity, higher dust temperature templates imply redshifts $z \sim 3$, with implied luminosities of $7 - 14 \times 10^{12}\ L_{\odot}$ for the sources we classify as good, while the lower temperature, lower luminosity templates imply redshifts closer to $z \sim 1$ with luminosities $1 - 2 \times 10^{12}\ L_{\odot}$. Noble *et al.* (2013) argued that lower temperature, lower redshift solutions were not compatible with the empirical temperature-luminosity relation derived by Roseboom *et al.* (2012) for *Herschel* selected sources. However, further work (*e.g.* Casey *et al.* 2012) has shown that there is a significant amount of scatter in this relation. This weakens any conclusion that can be drawn from such an analysis. While higher redshifts for our sources are still somewhat favored by the T-L relation in Casey *et al.* (2012) the possibility that some of our sources are cool outliers in this relation cannot be discounted. Our analysis of the optical/near-IR SED of the one source where we have a clear identification, LABOCA_2 seems to favor higher redshifts, but without enough precision to differentiate between $z \sim 2$ and $z \sim 3$.

Clearly, future SMA observations of targets in this and similar fields using SWARM will likely be able to detect these candidate cluster members and help determine accurate positions (and possibly redshifts!) for the highly unresolved LABOCA and SCUBA2 sources. With precise positions in hand, further followup observations including optical/near-IR imaging and spectroscopy are possible which would firmly establish the nature of the overdensity and confirm the tantalising possibility that this might be a galaxy cluster/protocluster at $z \sim 3.26$.

REFERENCES:

- Bradford, C. M., et al., 2004, Proceeedings of the SPIE, 5498, 257
- Bussmann R. S., et al., 2013, ApJ, 779, 25
- Casey C. M., et al., 2012, ApJ, 761, 140
- Casey C. M., et al., 2015, ApJ, 808, L33
- Chapman S. C., Blain A. W., Smail I., Ivison R. J., 2005, ApJ, 622, 772
- Clements D. L., et al., 2008, MNRAS, 387, 247
- Dannerbauer H., et al., 2014, A&A, 570, AA55
- Dempsey J. T., et al., 2013, MNRAS, 430, 2534
- Fu, H., et al., 2012, ApJ., 753, 134
- Gusten R., Philipp S. D., Weiss A., Klein B., 2006, A&A, 454, L115
- Harris A. I., et al., 2012, ApJ, 752, 152
- Holland W. S., et al., 2013, MNRAS, 430, 2513
- Ma C. J., et al., 2015, arXiv, arXiv:1504.06630
- Michalowski M., Hjorth J., Watson D., 2010, A&A, 514, A67
- Negrello, M., et al., 2010, Science, 330, 800
- Noble A. G., et al., 2013, MNRAS, 436, L40
- Pilbratt, G. L., et al., 2010, A\&A, 518, L1

32 GHZ SWARM BANDWIDTH IS NOW AVAILABLE FOR SCIENCE

the SWARM Development Team

After a heroic effort to complete the fourth quadrant of SWARM and the 10-12 GHz block downconverter before Christmas 2016, and following a series of tests and the squashing of one or two bugs, the SWARM Development Team is very pleased to announce that the SMA now offers up to 32 GHz of processed bandwidth — twice the processed bandwidth of ALMA — which can be configured for 32 GHz of instantaneous on sky frequency coverage or 16 GHz of frequency coverage with dual polarization. Moreover, all observations automatically produce 140 kHz uniform spectral resolution across that full band—yielding about 13 million channels for each scan—all of which are archived at the CfA Radio Telescope Data Center (RTDC). The availability of 32 GHz of processed bandwidth greatly improves observing efficiency or sensitivity for both the SMA and the SMA baselines of the Event Horizon Telescope VLBI. The high spectral resolution across the entire bandwidth improves the flexibility of post-observing analysis and potentially the usefulness of the archived data for future scientific investigations.

Options for configuring the improved bandwidth include: 16 GHz single polarization in each of two distinct atmospheric windows; 32 GHz in a single contiguous window; or dual polarization with 16 GHz of sky coverage in either the 230 or the 345 GHz window. **Figure 1**, a spectrum of Orion BN/KL, shows how we can obtain 32 GHz of contiguous sky coverage by choosing an offset of 8 GHz between the center frequencies of our double-sideband receivers. A similar setting is available for the 345 and 400 GHz receivers. We expect this to be very useful for line surveys. For dual polarization, two receivers are tuned with exactly overlapping bands. The VLBI mode for the EHT array covers 16 GHz (64 Gbps).

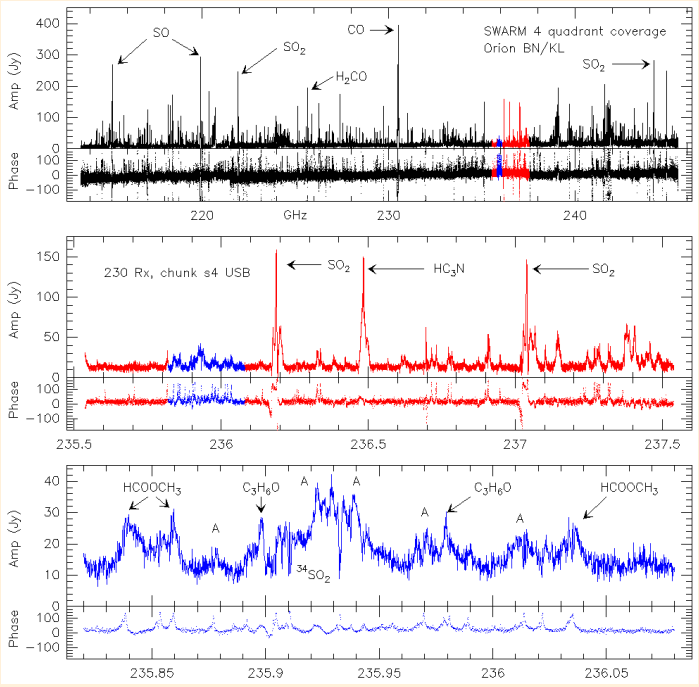

Figure 1: The top figure shows the full 32 GHz instantaneous spectral coverage we obtain from the completed, four quadrant SWARM correlator. To obtain continuous spectral coverage, the 240 GHz receiver set was tuned 8 GHz higher in sky frequency than the 230 GHz receiver set. Since each sideband of each receiver produces 8 GHz of spectral coverage, and since the hole in coverage between the LSB and USB of each receiver set is also 8 GHz, tuning the two receiver sets in this way interleaves the sidebands, and produces gap-free coverage. The 345 GHz and 400 GHz receiver sets can be similarly offset, to provide 32 GHz of coverage in the 345 GHz window. The red and blue portion of the top figure represents the USB of a single receiver and SWARM quadrant. That quadrant is shown alone in the middle figure. The bottom figure shows a portion of that same quadrant, and highlights the high (~140 KHz) resolution SWARM provides throughout its 32 GHz coverage. Spectral lines labelled A are from $^{13}CH_3OH$. SWARM produces nearly 1/4 million usable spectral channels on each baseline.

While it is well understood that only a subset of spectral line observations require this exquisite resolution, we believe great value may lie in "off-label" use of archived data, for science the original PI may not have envisaged. For example, with our previous correlator, an observation could cover only a few spectral lines at high resolution. Now the data include high resolution on all spectral lines in the bandwidth – even those that were not science targets of the original observation. For those projects requiring high resolution of only a few spectral lines, a fast "reChunker" software tool can quickly reduce the size of the data set by reprocessing the remaining data to lower resolution for use as continuum and in calibration.

For those who wish to look under the hood for more information on how SWARM works, please see recent papers by Primiani, et al ("SWARM: A 32 GHz Correlator and VLBI Beamformer for the Submillimeter Array", Journal of Astronomical Instrumentation, Volume 5, no 4, December 2016) and an IEEE paper on the VLBI phased array by Young et al. ("Performance Assessment of an Adaptive Beamformer for the Submillimeter Array", Proceedings of the IEEE International Symposium on Phased Array Systems & Technology, 18-21 October 2016, Waltham, MA).

Much thanks is due for the hard work of SMA staff in Hawaii and Cambridge. The best reward for the SWARM Development Team is seeing how the creativity and industry of the community of SMA observers can produce amazing scientific results enabled by this new capability. The SAO Digital Signal Processing team is not sitting on its laurels. Work is proceeding to quadruple the bandwidth of the SMA again in the context of wSMA, and to couple our DSP developments and similar back end features to ALMA.

INTRODUCING THE wSMA – A MAJOR UPGRADE TO THE SMA RECEIVER SYSTEMS

Paul Grimes, Edward Tong, Scott Paine, Lingzhen Zeng and Ray Blundell

The current SMA receiver systems were designed in the mid-1990s and have been operating for more than fifteen years. With continuous upgrades to the receiver inserts installed within the cryostats, the deployment of the SWARM correlator, expansion of the IF signal transport bandwidth via improvements to the analog IF signal processing hardware, and many other enhancements, the SMA currently greatly outperforms its original specifications in sensitivity, instantaneous bandwidth, and the availability of observing modes such as full-Stokes polarization and dual frequency operation.

Further significant upgrades to the SMA performance are scientifically compelling, but will require major changes to the receivers and IF signal transport systems. Additionally, the SMA must address the purely practical problem that the cryogenic refrigerators that cool the SMA receivers are near the end of their service life. Repair parts are limited to stocks held by the SMA, and equivalent replacement cryocoolers are not commercially available.

We have thus decided to undertake a major upgrade of the SMA's receiver systems that will significantly increase the sensitivity of the SMA by reducing receiver noise and by increasing the SMA's instantaneous bandwidth by a factor of two.

The major subsystems that will form the wSMA include a new cryostat housing upgraded receiver cartridges, upgraded local oscillator units, an upgraded signal transmission system, and an expansion of the SWARM correlator system. The cryostat will be cooled by a low-maintenance pulse-tube cryocooler. Two dual-polarization receiver cartridges will cover approximately the same sky frequencies as the current three 200 GHz, 240 GHz and 300 GHz single-polarization receivers; the low-band receiver will be fed by an LO unit covering 210-270 GHz, and the high-band receiver will be fed by an LO covering 280-360 GHz. With a receiver IF band of 4-18 GHz, this will enable continuous frequency coverage from 192 GHz to 378 GHz. A schematic of the new receiver concept is shown in Fig. 1, and a CAD concept model in Fig. 2.

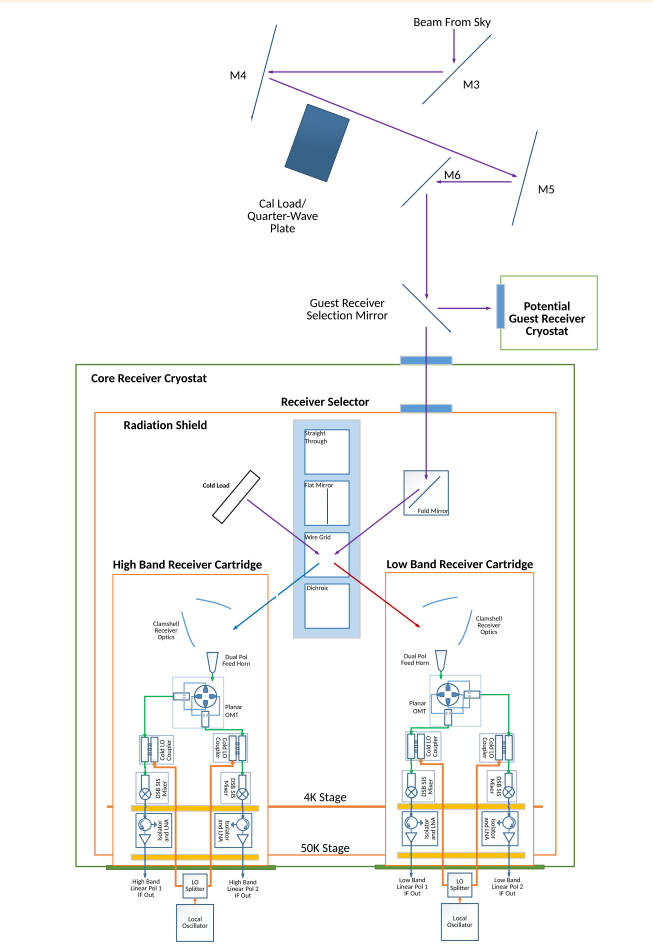

Figure 1: Schematic of the new SMA receiver system. A new receiver cryostat holds two dual polarization receiver inserts and the cooled receiver selection optics.

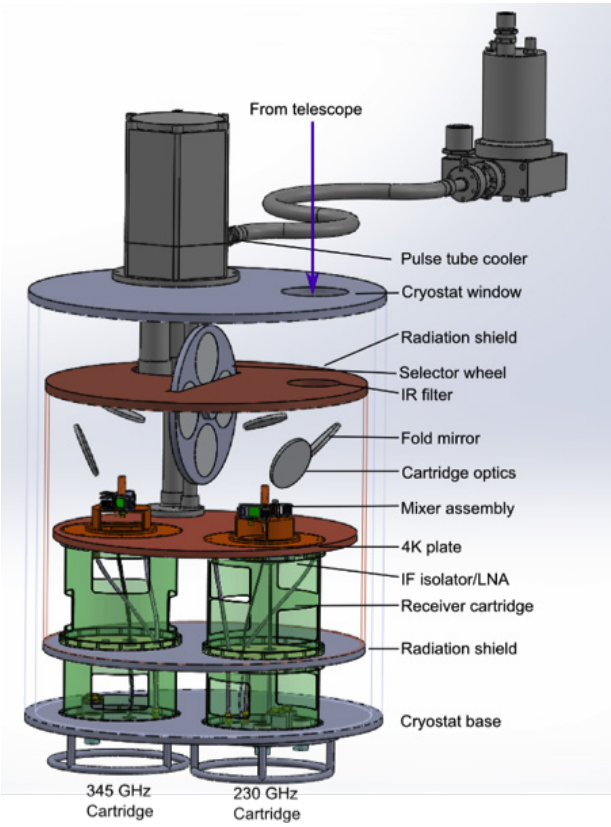

Figure 2. CAD Concept model of the wSMA receiver cryostat (cryostat and radiation shield walls hidden). The beam from the telescope enters from the top of the cryostat, and is reflected through 90° to the receiver selector wheel, which sends it to either of the two receiver inserts. The receiver inserts are inserted from the base of the cryostat.

Each receiver cartridge will contain a dual-polarization, double-sideband, front end incorporating a single feedhorn and an orthomode transducer polarization splitter feeding two SIS mixers. The use of a common feedhorn and optics for both polarizations will ensure the coalignment of the two polarization beams on the sky, significantly improving the polarimetric performance of the SMA. Local oscillator signals will be coupled to the mixers via cold waveguide injection. This will result in lower room temperature losses than the current quasioptical injection scheme, reducing receiver noise.

The active receiver or receivers will be selected using a selector wheel mounted within the cryostat and cooled to 50K, further reducing warm losses in the optical path compared with the current room-temperature scheme. The selector wheel will allow both polarizations from the sky to be directed to either of the two receiver cartridges for dual-polarization observations, or for the two polarizations to be split by a wire grid for dual frequency observing with one polarization active in each receiver cartridge. A fourth observing mode will be possible using a dichroic splitter, which will split the incoming signal beam by frequency, allowing dual polarization observing by both receiver bands simultaneously, albeit with some limitations on performance. A 50 K cold calibration load included within the cryostat will be viewed by polarizations that are not directed towards the sky. Together with the existing warm calibration load, this will improve receiver calibration and optimization.

To support the substantial increase in the receiver IF bandwidth, as well as the possibility to observe with four mixers simultaneously, upgrades will be made to the fiber optic system that carries reference and timing signals from the control building to the individual antennas, and the IF output signals from the receivers back to the SWARM correlator. Processing the increased IF bandwidth will require more correlator capacity, which will be supplied by installing additional segments of the SWARM correlator.

We are planning to carry out the wSMA upgrade over the next 3 years. In 2017, the fiber optic systems will be upgraded while receiver development and testing proceeds in Cambridge and Taipei. We aim to test the first two prototype receiver systems on two antennas in the first half of 2018, before deploying the remaining receiver systems from late 2018 through 2019. The additional correlator capacity will be installed in 2019.

Throughout the upgrade process, we will ensure that the SMA continues operations with a minimum of 6 antennas; upgrading each antenna will require time in the hangar while the work of installing the new receivers is carried out. The new receiver systems will be backwards compatible with the current receiver systems and we expect that observations will not be significantly impacted.

The wSMA upgrade will enable new observing modes and enhanced sensitivity. The observing modes and expected performance of the wSMA following the upgrade are compared with the current SMA in Table 1.

Since the new receiver system will be physically smaller than the existing system, this upgrade will also open up more space in the receiver cabin which may be used in the future to host guest or development instruments. Possibilities include instruments for higher frequency observations or to demonstrate new technologies such as multibeam SIS receivers for interferometry.

	Current Receiver		New Receiver	
Receiver Bands	200	186-242 GHz	230	210-270 GHz
	240	210-270 GHz		
	300	271-349 GHz	345	280-360 GHz
	400	330-420 GHz		
IF Bandwidth	4 - 12 GHz		4-18 GHz	
Receiver Selections	200+240 Dual polarization 210-242 GHz		230 Dual polarization over full band	
	300+400 Dual polarization 330-349 GHz		345 Dual polarization over full band	
	240+300 Dual frequency		230+345 Dual pol, dual freq with dichroic or time sharing. Single pol, dual freq with wire grid	
	200+400 Dual frequency			
Receiver Noise Temperature	200	50-55 K	230	40 K
	240	50-60 K		
	300	70-80 K	345	55 K
	400	75-85 K		
Interferometer Sensitivity in typical observing conditions (4mm PWV for 230 GHz, 2.5mm PWV for 345 GHz)				
System Temperature	200	168 K	230	152 K
	240	176 K		
	300	349 K	345	308 K
	400	359 K		
Continuum Sensitvity 6 hours on source	200/240	0.46 mJy/beam	230	0.32 mJy/beam
	300/400	0.91 mJy/beam	345	0.63 mJy/beam
Interferometer Sensitivity in best 10% weather (1mm PWV for both 230 GHz and 345 GHz)				
System Temperature	200	100 K	230	86 K
	240	106 K		
	300	197 K	345	166 K
	400	205 K		
Continuum Sensitvity 6 hours on source	200/240	0.30 mJy/beam	230	0.21 mJy/beam
	300/400	0.53 mJy/beam	345	0.36 mJy/beam

Table 1: Comparison of current SMA receiver specifications with the upgraded wSMA.

CALL FOR SMA SCIENCE OBSERVING PROPOSALS

The joint CfA-ASIAA SMA Time Allocation Committee (TAC) solicits proposals for observations for the period May 16, 2017 - Nov 15, 2017 (2017A semester). The deadline for submitting proposals is Feb 8, 2017.

The SMA Observer Center website (http://sma1.sma.hawaii.edu/proposing.html) is expected to open for proposal submission on Jan. 18, 2017.

ASIAA WORKSHOP - "SMA SCIENCE IN THE NEW DECADE"

The Aacademia Sinica Institute for Astronomy and Astrophyics hosted a workshop on "SMA Science in the Next Decade", October 27-28, 2016. This workshop provided a forum for astronomers from the SMA collaboration and user community to promote, discuss, and elaborate on science opportunities with an upgraded wideband SMA (wSMA) that aims to process 32 GHz in two polarizations, from two receiver bands simultaneously. There were 86 registered participants, including 54 from Taiwan, 16 from SAO, and 16 from elsewhere around the world. A lively program of 21 invited talks and 3 discussion sessions focused on the impact of new wSMA capabilities on a wide range of science topics, from comets to the high redshift universe. The breadth of the program underscored the importance of high angular resolution millimeter and submillimeter observations in modern astrophysics. Also discussed were technical issues, large observing projects, and the broader context of other facilities operating at these wavelengths, including ALMA, IRAM/NOEMA and JCMT. An additional 14 shorter contributed talks and 10 posters, mostly from younger scientists, described recent science results. Everyone also enjoyed a tremendous traditional Chinese banquet at a nearby restaurant. The intellectual content of the formal program is captured in the presentations posted on the conference web pages. At least as important, the numerous breaks and shared meals enabled informal conversations throughout the workshop to conduct science, and to develop and enhance new scientific collaborations. Thanks to all of the organizers for a very successful meeting.

Site link:

http://events.asiaa.sinica.edu.tw/workshop/20161027/index.php

RIMA ROCHA RETIRES AFTER 17 YEARS

Rima Rocha retired at the end of August, just over 17 years after she joined the SMA in Hilo. She arrived during a busy period, with the staff expanding to support antenna assembly and nascent array operations. Soon after her arrival, the first fringes were obtained with two antennas on Maunakea, a major milestone. She was a part of every subsequent milestone and event. Rima was a pillar of the support staff. She attentively arranged travel for observers and other visitors, tirelessly kept the vehicles running, and shipped countless receiver and telescope parts back and forth. Always cheerful, she was enthusiastic about new assignments and challenges.

Thank you, Rima, for supporting the SMA all these years. Happy Retirement!

SHIRIN MONTAZERI WINS FIRST PLACE IN THE BEST STUDENT PAPER PRIZE AT THE 2016 APPLIED SUPERCONDUCTIVITY CONFERENCE

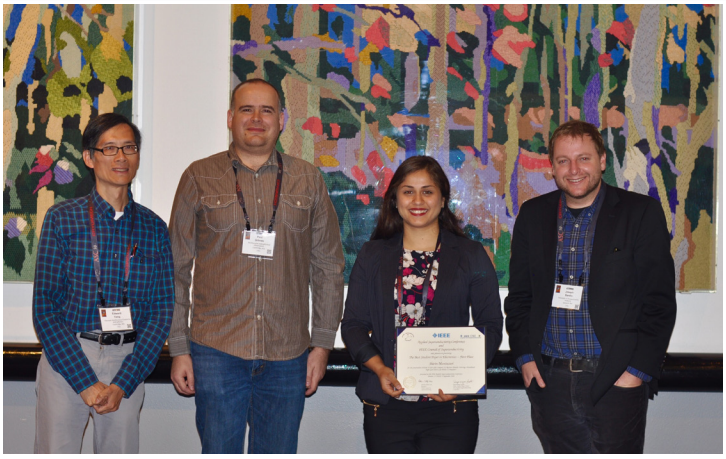

Shirin Montazeri, a student at UMass Amherst, has won first place in the Best Student Paper Prize at the 2016 Applied Superconductivity Conference held in Denver earlier this month for the work she has done in the Receiver Lab at SAO. The winning paper is: A 220-GHz Compact SIS Receiver Module Utilizing a Broadband High-Gain Ultra-Low-Power IF Amplifier, Shirin Montazeri, Paul Grimes, Edward Tong, and Joseph Bardin.

Link to conference: http://ascinc.org/conference-program/paper-contest/

PROPOSAL STATISTICS 2016B (16 NOV 2016 - 15 MAY 2017)

The SMA received a total of 82 proposals (SAO 59) requesting observing time in the 2016B semester. The proposals received by the joint SAO and ASIAA Time Allocation Committee are divided among science categories as follows:

Category	Proposals
low/intermediate mass star formation, cores	20
submm/hi-z galaxies	18
high mass (OB) star formation, cores	11
local galaxies, starbursts, AGN	10
GRB, SN, high energy	5
protoplanetary, transition, debris disks	5
UH	5
evolved stars, AGB, PPN	4
solar system	3
galactic center	1

TRACK ALLOCATIONS BY WEATHER REQUIREMENT (ALL PARTNERS):

PWV[1]	SAO	ASIAA	UH[2]
< 4.0mm	13A + 43B	8A + 4B	12
< 2.5mm	14A + 33B	2A + 7B	10
< 1.0mm	2A + 0B	0A + 0B	0
Total	**29A + 76B**	**10A + 11B**	**22**

(1) Precipitable water vapor required for the observations.

(2) UH does not list As and Bs.

TOP-RANKED SAO AND ASIAA PROPOSALS – 2016B SEMESTER

The following is the listing of all SAO and ASIAA proposals with at least a partial A ranking with the names and affiliations of the principal investigators.

EVOLVED STARS, AGB, PPN

Peter Scicluna, ASIAA
Grain growth in Herschel selected post-AGB stars with discs

GALACTIC CENTER

Hau-Yu Baobab Liu, ESO-Garching
First Submillimeter Interferometric Polarimetry of the Galactic Circumnuclear Ring

GRB, SN, HIGH ENERGY

Yuji Urata, NCU/ASIAA
Search for Bright submm GRB afterglows Toward First Radio Polarimetry

HIGH MASS (OB) STAR FORMATION, CORES

Keping Qiu, School of Astronomy and Space Science, Nanjing University
Mapping the molecular bullets in HH80-81: the first proper motion experiment for EHV molecular gas in a high-mass protostar

Qizhou Zhang, CfA
Role of Magnetic Fields in the Early Phase of Massive Star Formation

Tao-Chung Ching, National Tsing Hua University, Taiwan
Pilot mosaic polarization observations in Orion BN/KL and W51

LOCAL GALAXIES, STARBURSTS, AGN

Geoffrey Bower, ASIAA
Variability Timescale of Low Luminosity AGN

Hsi-an Pan, ASIAA
The Impact of Minor Merger on Galaxy Evolution and Massive Star Formation Environment: an indispensable piece of cosmic galaxy evolution framework

LOW/INTERMEDIATE MASS STAR FORMATION, CORES

Elizabeth Artur de la Villarmois, StarPlan - Niels Bohr Institut
Unlocking the protostellar carbon chemistry with SWARM

Lars Kristensen, Center for Star & Planet Formation, Niels Bohr Institute, Copenhagen University
Ice to gas: determining the desorption efficiency of methanol

Shaye Storm, SAO
Star Clusters in Formation: Probing their Young Stellar Systems

PROTOPLANETARY, TRANSITION, DEBRIS DISKS

David Wilner, CfA
The 61 Vir Planetary System Debris Disk

SOLAR SYSTEM

Charlie Qi, CfA
Catching an Outbursting Comet

SUBMM/HI-Z GALAXIES

Garrett "Karto" Keating, SMA/SAO
Charting the Cosmic History of Molecular Gas with Intensity Mapping

Iván Oteo Gómez, University of Edinburgh / ESO
The molecular gas of low-z submm galaxies

Min Yun, University of Massachusetts
Probing Dense Gas Powering SF/AGN Activities in High-z SMGs using Lensing

Yoshiki Toba, ASIAA
Search for most infrared luminous galaxy in the Universe

ALL SAO PROPOSALS - 2016A SEMESTER

The following is the listing of all SAO proposals observed in the 2016A semester (16 May 2016 - 15 Nov 2016)

Hector Arce, Yale University
Revealing the Physical Structure of a Class I Disk

Akos Bogdan, CfA
Tracing the Evolution of the Closest Supermassive Black Hole Binary

Scott Chapman, Dalhousie University
Characterizing the bright submillimeter galaxy population with SMA in SCUBA-2 CLS fields

Tao-Chung Ching, National Tsing Hua University, Taiwan
Pilot mosaic polarization observations in Orion BN/KL and W51

Rumpa Choudhury, MPIfR
Do expanding bubbles pave the way for the next generation of high-mass pre stellar cores?

Asantha Cooray, University of California, Irvine
High Resolution Imaging of Rarest and Brightest Herschel-selected sub-millimeter Galaxies

Josep Miquel Girart, CfA
Observing the onset of outflow collimation in a massive protostar

Mark Gurwell, CfA
The Surface and Atmosphere of Triton

Jorma Harju, Department of Physics, University of Helsinki
A stellar cluster in formation - filamentary inflow induced by colliding filaments

J Hatchell, University of Exeter
FHSC candidates in Serpens South

Naomi Hirano, ASIAA
Is the L1448C(N) protostellar jet "extremely active"? -- three dimensional kinematic structure probed by proper motions

Taylor Hogge, Boston University
Mapping Outflows in the Extreme High-mass Star-forming Region G23.33-0.30

Li-Yen Hsu, University of Hawaii
Characterizing faint submillimeter galaxies with cluster lensing

Chat Hull, CfA
Cepheus Polarization Survey: a Pilot Study

Carmen Juarez, Institute of Space Sciences (IEEC-CSIC)
Assessing the role of magnetic fields in a filament with super-Jeans fragmentation

Atish Kamble, CfA
SMA Observations of young, nearby SN 2016iae

Tomasz Kaminski, CfA
Thermal echoes at submillimeter wavelengths

Sheng-Yuan Liu, ASIAA
Exploring the Molecular Content of the Infrared Jet-Outflow System in the Rare O-Type Protostar W42-MME

Hau-Yu Baobab Liu, ESO-Garching
First Submillimeter Interferometric Polarimetry of the Galactic Circumnuclear Ring

Wen-Ping Lo, ASIAA
Verify the black hole magnetosphere model for origin of very-high-energy gamma-ray emission in IC 310 with SMA polarimetry

Michael McCollough, CfA
Cygnus X-3's Little Friend: Understanding the nature of the most distant observed Bok Globule and its jets

Nicole Nesvadba, Institut d'Astrophysique Spatiale Orsay (France)
Zooming in onto star formation in the brightest gravitationally lensed galaxies from the Planck all-sky survey

Nimesh Patel, CfA
Chemical Evolution from AGB to PN: A Spectral-line Survey of CRL 2688 and NGC 7027

Glen Petitpas, CfA
The Beautiful and Enigmatic Spiral Galaxy NGC 7331

Charlie Qi, CfA
The Primary Volatile Composition of a Dynamically New Comet - C/2013 X1 (PanSTARRS)

Keping Qiu, Nanjing University
Completing the SMA survey of massive cores in Cygnus X

Howard Smith, CfA
Understanding How a Black Hole Feeds: SMA Observations of SgrA Simultaneous with Spitzer and Chandra*

John Tobin, University of Oklahoma
Characterizing the Chemical Impact of Episodic Accretion

Yuji Urata, NCU/ASIAA
Search for Bright submm afterglows Associated with Gamma-Ray Bursts

Nienke van der Marel, University of Hawaii
Targeting the CN emission in protoplanetary disks: a measure of the UV field

Johan van der Walt, North-West University
Evolutionary Stage Implications of Periodic Methanol Maser Sources

Jonathan Williams, University of Hawaii
The radial temperature gradient of an edge-on disk

Jonathan Williams, University of Hawaii
Imaging debris-disk structure with the SMA

David Wilner, CfA
The HR 8799 Planetary System Debris DIsk

Luis Zapata, CRyA-UNAM
Resolving the engine of DG TAU B at submillimeter wavelengths

Qizhou Zhang, CfA
Constraining angular momenta in the disk wind using recombination masers in MWC349A

RECENT PUBLICATIONS

Title: Search for aluminium monoxide in the winds of oxygen-rich AGB stars
Authors: De Beck, E.; Decin, L.; Ramstedt, S.; Olofsson, H.; Menten, K. M.; Patel, N. A.; Vlemmings, W. H. T.
Publication: *eprint arXiv:1611.05409*
Publication Date: 11/2016
Abstract: http://adsabs.harvard.edu/abs/2016arXiv161105409D

Title: The Herschel-ATLAS: a sample of 500 μm-selected lensed galaxies over 600 deg^2
Authors: Negrello, M.; Amber, S.; Amvrosiadis, A.; Cai, Z.-Y.; Lapi, A.; Gonzalez-Nuevo, J.; De Zotti, G.; Furlanetto, C.; Maddox, S. J.; Allen, M.; Bakx, T.; Bussmann, R. S.; Cooray, A.; Covone, G.; Danese, L.; Dannerbauer, H.; Fu, H.; Greenslade, J.; Gurwell, M.; Hopwood, R.; Koopmans, L. V. E.; Napolitano, N.; Nayyeri, H.; Omont, A.; Petrillo, C. E.; Riechers, D. A.; Serjeant, S.; Tortora, C.; Valiante, E.; Verdoes Kleijn, G.; Vernardos, G.; Wardlow, J. L.; Baes, M.; Baker, A. J.; Bourne, N.; Clements, D.; Crawford, S. M.; Dye, S.; Dunne, L.; Eales, S.; Ivison, R. J.; Marchetti, L.; Michałowski, M. J.; Smith, M. W. L.; Vaccari, M.; van der Werf, P.
Publication: *Monthly Notices of the Royal Astronomical Society, Volume 465, Issue 3, p.3558-3580 (MNRAS Homepage)*
Publication Date: 03/2017
Abstract: http://adsabs.harvard.edu/abs/2017MNRAS.465.3558N

Title: SWARM: A 32 GHz Correlator and VLBI Beamformer for the Submillimeter Array
Authors: Primiani, Rurik A.; Young, Kenneth H.; Young, André; Patel, Nimesh; Wilson, Robert W.; Vertatschitsch, Laura; Chitwood, Billie B.; Srinivasan, Ranjani; MacMahon, David; Weintroub, Jonathan
Publication: *eprint arXiv:1611.02596*
Publication Date: 11/2016
Abstract: http://adsabs.harvard.edu/abs/2016arXiv161102596P

Title: Tracing Infall and Rotation along the Outflow Cavity Walls of the L483 Protostellar Envelope
Authors: Leung, Gigi Y. C.; Lim, Jeremy; Takakuwa, Shigehisa
Publication: *The Astrophysical Journal, Volume 833, Issue 1, article id. 55, 19 pp. (2016). (ApJ Homepage)*
Publication Date: 11/2016
Abstract: http://adsabs.harvard.edu/abs/2016ApJ...833...55L

Title: The Multiple Young Stellar Objects of HBC 515: An X-ray and Millimeter-wave Imaging Study in (Pre-main Sequence) Diversity
Authors: Principe, D. A.; Sacco, G. G.; Kastner, J. H.; Wilner, D.; Stelzer, B.; Micela, G.
Publication: *eprint arXiv:1610.03851*
Publication Date: 10/2016
Abstract: http://adsabs.harvard.edu/abs/2016arXiv161003851P

Title: The Galactic Center Molecular Cloud Survey. II. A Lack of Dense Gas & Cloud Evolution along Galactic Center Orbits
Authors: Kauffmann, Jens; Pillai, Thushara; Zhang, Qizhou; Menten, Karl M.; Goldsmith, Paul F.; Lu, Xing; Guzmán, Andrés E.; Schmiedeke, Anika
Publication: *eprint arXiv:1610.03502*
Publication Date: 10/2016
Abstract: http://adsabs.harvard.edu/abs/2016arXiv161003502K

Title: The Galactic Center Molecular Cloud Survey. I. A Steep Linewidth-Size Relation & Suppression of Star Formation
Authors: Kauffmann, Jens; Pillai, Thushara; Zhang, Qizhou; Menten, Karl M.; Goldsmith, Paul F.; Lu, Xing; Guzmán, Andrés E.
Publication: *eprint arXiv:1610.03499*
Publication Date: 10/2016
Abstract: http://adsabs.harvard.edu/abs/2016arXiv161003499K

Title: Cygnus X-3: Its Little Friend's Counterpart, the Distance to Cygnus X-3, and Outflows/Jets
Authors: McCollough, M. L.; Corrales, L.; Dunham, M. M.
Publication: *The Astrophysical Journal Letters, Volume 830, Issue 2, article id. L36, 5 pp. (2016). (ApJL Homepage)*
Publication Date: 10/2016
Abstract: http://adsabs.harvard.edu/abs/2016ApJ...830L..36M

Title: Interpreting observations of edge-on gravitationally unstable accretion flows
Authors: Liu, Hauyu Baobab
Publication: *eprint arXiv:1609.07296*
Publication Date: 09/2016
Abstract: http://adsabs.harvard.edu/abs/2016arXiv160907296L

Title: Clumpy and Extended Starbursts in the Brightest Unlensed Submillimeter Galaxies
Authors: Iono, Daisuke; Yun, Min S.; Aretxaga, Itziar; Hatsukade, Bunyo; Hughes, David; Ikarashi, Soh; Izumi, Takuma; Kawabe, Ryohei; Kohno, Kotaro; Lee, Minju; Matsuda, Yuichi; Nakanishi, Kouichiro; Saito, Toshiki; Tamura, Yoichi; Ueda, Junko; Umehata, Hideki; Wilson, Grant; Michiyama, Tomonari; Ando, Misaki
Publication: *The Astrophysical Journal Letters, Volume 829, Issue 1, article id. L10, 6 pp. (2016). (ApJL Homepage)*
Publication Date: 09/2016
Abstract: http://adsabs.harvard.edu/abs/2016ApJ...829L..10I

Title: 880 μm SMA Polarization Observations of the Quasar 3C 286
Authors: Hull, Charles L. H.; Girart, Josep M.; Zhang, Qizhou
Publication: *The Astrophysical Journal, Volume 830, Issue 2, article id. 124, 4 pp. (2016). (ApJ Homepage)*
Publication Date: 10/2016
Abstract: http://adsabs.harvard.edu/abs/2016arXiv160806283H

Title: G11.92-0.61 MM1: a Keplerian disc around a massive young proto-O star
Authors: Ilee, J. D.; Cyganowski, C. J.; Nazari, P.; Hunter, T. R.; Brogan, C. L.; Forgan, D. H.; Zhang, Q.
Publication: *Monthly Notices of the Royal Astronomical Society, Volume 462, Issue 4, p.4386-4401 (MNRAS Homepage)*
Publication Date: 11/2016
Abstract: http://adsabs.harvard.edu/abs/2016MNRAS.462.4386I

Title: The Molecular Baryon Cycle of M82
Authors: Chisholm, John; Matsushita, Satoki
Publication: *The Astrophysical Journal, Volume 830, Issue 2, article id. 72, 15 pp. (2016). (ApJ Homepage)*
Publication Date: 10/2016
Abstract: http://adsabs.harvard.edu/abs/2016ApJ...830...72C

Title: The Connection between the Radio Jet and the γ-ray Emission in the Radio Galaxy 3C 120 and the Blazar CTA 102
Authors: Casadio, Carolina; Gómez, José; Jorstad, Svetlana; Marscher, Alan; Grandi, Paola; Larionov, Valeri; Lister, Matthew; Smith, Paul; Gurwell, Mark; Lähteenmäki, Anne; Agudo, Iván; Molina, Sol; Bala, Vishal; Joshi, Manasvita; Taylor, Brian; Williamson, Karen; Kovalev, Yuri; Savolainen, Tuomas; Pushkarev, Alexander; Arkharov, Arkady; Blinov, Dmitry; Borman, George; Di Paola, Andrea; Grishina, Tatiana; Hagen-Thorn, Vladimir; Itoh, Ryosuke; Kopatskaya, Evgenia; Larionova, Elena; Larionova, Liudmila; Morozova, Daria; Rastorgueva-Foi, Elizaveta; Sergeev, Sergey; Tornikoski, Merja; Troitsky, Ivan; Thum, Clemens; Wiesemeyer, Helmut
Publication: *Galaxies, vol. 4, issue 4, p. 34*
Publication Date: 09/2016
Abstract: http://adsabs.harvard.edu/abs/2016Galax...4...34C

Title:	Optical Outburst of the Blazar S4 0954+658 in Early 2015
Authors:	Morozova, Daria; Larionov, Valeri; Jorstad, Svetlana; Marscher, Alan; Troitskaya, Yulia; Troitskiy, Ivan; Blinov, Dmitriy; Borman, Georg; Gurwell, Mark
Publication:	*Galaxies, vol. 4, issue 3, p. 24*
Publication Date:	09/2016
Abstract:	http://adsabs.harvard.edu/abs/2016Galax...4...24M

Title:	The structure and early evolution of massive star forming regions. Substructure in the infrared dark cloud SDC13
Authors:	McGuire, C.; Fuller, G. A.; Peretto, N.; Zhang, Q.; Traficante, A.; Avison, A.; Jimenez-Serra, I.
Publication:	*Astronomy & Astrophysics, Volume 594, id.A118, 13 pp. (A&A Homepage)*
Publication Date:	10/2016
Abstract:	http://adsabs.harvard.edu/abs/2016arXiv160707851M

Title:	Multiwavelength study of the low-luminosity outbursting young star HBC 722
Authors:	Kóspál, Á.; Ábrahám, P.; Acosta-Pulido, J. A.; Dunham, M. M.; García-Álvarez, D.; Hogerheijde, M. R.; Kun, M.; Moór, A.; Farkas, A.; Hajdu, G.; Hodosán, G.; Kovács, T.; Kriskovics, L.; Marton, G.; Molnár, L.; Pál, A.; Sárneczky, K.; Sódor, Á.; Szakáts, R.; Szalai, T.; Szegedi-Elek, E.; Szing, A.; Tóth, I.; Vida, K.; Vinkó, J.
Publication:	*Astronomy & Astrophysics, Volume 596, id.A52, 15 pp. (A&A Homepage)*
Publication Date:	11/2016
Abstract:	http://adsabs.harvard.edu/abs/2016arXiv160705925K

Title:	Spiral Structure and Differential Dust Size Distribution in the LKHα 330 Disk
Authors:	Akiyama, Eiji; Hashimoto, Jun; baobabu Liu, Hauyu; i-hsiu Li, Jennifer; Bonnefoy, Michael; Dong, Ruobing; Hasegawa, Yasuhiro; Henning, Thomas; Sitko, Michael L.; Janson, Markus; Feldt, Markus; Wisniewski, John; Kudo, Tomoyuki; Kusakabe, Nobuhiko; Tsukagoshi, Takashi; Momose, Munetake; Muto, Takayuki; Taki, Tetsuo; Kuzuhara, Masayuki; Satoshi, Mayama; Takami, Michihiro; Ohashi, Nagayoshi; Grady, Carol A.; Kwon, Jungmi; Thalmann, Christian; Abe, Lyu; Brandner, Wolfgang; Brandt, Timothy D.; Carson, Joseph C.; Egner, Sebastian; Goto, Miwa; Guyon, Olivier; Hayano, Yutaka; Hayashi, Masahiko; Hayashi, Saeko S.; Hodapp, Klaus W.; Ishii, Miki; Iye, Masanori; Knapp, Gillian R.; Kandori, Ryo; Matsuo, Taro; Mcelwain, Michael W.; Miyama, Shoken; Morino, Jun-Ichi; Moro-Martin, Amaya; Nishimura, Tetsuo; Pyo, Tae-Soo; Serabyn, Eugene; Suenaga, Takuya; Suto, Hiroshi; Suzuki, Ryuji; Takahashi, Yasuhiro H.; Takato, Naruhisa; Terada, Hiroshi; Tomono, Daigo; Turner, Edwin L.; Watanabe, Makoto; Yamada, Toru; Takami, Hideki; Usuda, Tomonori; Tamura, Motohide
Publication:	*The Astronomical Journal, Volume 152, Issue 6, article id. 222, 7 pp. (2016). (AJ Homepage)*
Publication Date:	12/2016
Abstract:	http://adsabs.harvard.edu/abs/2016arXiv160704708A

Title:	SMA observations towards the compact, short-lived bipolar water maser outflow in the LkHα234 region
Authors:	Girart, J. M.; Torrelles, J. M.; Estalella, R.; Curiel, S.; Anglada, G.; Gómez, J. F.; Carrasco-González, C.; Cantó, J.; Rodríguez, L. F.; Patel, N. A.; Trinidad, M. A.
Publication:	*Monthly Notices of the Royal Astronomical Society, Volume 462, Issue 1, p.352-361 (MNRAS Homepage)*
Publication Date:	10/2016
Abstract:	http://adsabs.harvard.edu/abs/2016MNRAS.462..352G

Title:	Location of Gamma-ray emission and magnetic field strengths in OJ 287
Authors:	Hodgson, J. A.; Krichbaum, T. P.; Marscher, A. P.; Jorstad, S. G.; Rani, B.; Marti-Vidal, I.; Bach, U.; Sanchez, S.; Bremer, M.; Lindqvist, M.; Uunila, M.; Kallunki, J.; Vicente, P.; Fuhrmann, L.; Angelakis, E.; Karamanavis, V.; Myserlis, I.; Nestoras, I.; Chidiac, C.; Sievers, A.; Gurwell, M.; Zensus, J. A.
Publication:	*eprint arXiv:1607.00725*
Publication Date:	Jul-16
Abstract:	http://adsabs.harvard.edu/abs/2016arXiv160700725H

Title: Planck intermediate results. XLV. Radio spectra of northern extragalactic radio sources
Authors: Planck Collaboration; Ade, P. A. R.; Aghanim, N.; Aller, H. D.; Aller, M. F.; Arnaud, M.; Aumont, J.; Baccigalupi, C.; Banday, A. J.; Barreiro, R. B.; Bartolo, N.; Battaner, E.; Benabed, K.; Benoit-Lévy, A.; Bernard, J.-P.; Bersanelli, M.; Bielewicz, P.; Bonaldi, A.; Bonavera, L.; Bond, J. R.; Borrill, J.; Bouchet, F. R.; Burigana, C.; Calabrese, E.; Catalano, A.; Chiang, H. C.; Christensen, P. R.; Clements, D. L.; Colombo, L. P. L.; Couchot, F.; Crill, B. P.; Curto, A.; Cuttaia, F.; Danese, L.; Davies, R. D.; Davis, R. J.; de Bernardis, P.; de Rosa, A.; de Zotti, G.; Delabrouille, J.; Dickinson, C.; Diego, J. M.; Dole, H.; Donzelli, S.; Doré, O.; Ducout, A.; Dupac, X.; Efstathiou, G.; Elsner, F.; Eriksen, H. K.; Finelli, F.; Forni, O.; Frailis, M.; Fraisse, A. A.; Franceschi, E.; Galeotta, S.; Galli, S.; Ganga, K.; Giard, M.; Giraud-Héraud, Y.; Gjerløw, E.; González-Nuevo, J.; Górski, K. M.; Gruppuso, A.; Gurwell, M. A.; Hansen, F. K.; Harrison, D. L.; Henrot-Versillé, S.; Hernández-Monteagudo, C.; Hildebrandt, S. R.; Hobson, M.; Hornstrup, A.; Hovatta, T.; Hovest, W.; Huffenberger, K. M.; Hurier, G.; Jaffe, A. H.; Jaffe, T. R.; Järvelä, E.; Keihänen, E.; Keskitalo, R.; Kisner, T. S.; Kneissl, R.; Knoche, J.; Kunz, M.; Kurki-Suonio, H.; Lähteenmäki, A.; Lamarre, J.-M.; Lasenby, A.; Lattanzi, M.; Lawrence, C. R.; Leonardi, R.; Levrier, F.; Liguori, M.; Lilje, P. B.; Linden-Vørnle, M.; López-Caniego, M.; Lubin, P. M.; Macías-Pérez, J. F.; Maffei, B.; Maino, D.; Mandolesi, N.; Maris, M.; Martin, P. G.; Martínez-González, E.; Masi, S.; Matarrese, S.; Max-Moerbeck, W.; Meinhold, P. R.; Melchiorri, A.; Mennella, A.; Migliaccio, M.; Mingaliev, M.; Miville-Deschênes, M.-A.; Moneti, A.; Montier, L.; Morgante, G.; Mortlock, D.; Munshi, D.; Murphy, J. A.; Nati, F.; Natoli, P.; Nieppola, E.; Noviello, F.; Novikov, D.; Novikov, I.; Pagano, L.; Pajot, F.; Paoletti, D.; Partridge, B.; Pasian, F.; Pearson, T. J.; Perdereau, O.; Perotto, L.; Pettorino, V.; Piacentini, F.; Piat, M.; Pierpaoli, E.; Plaszczynski, S.; Pointecouteau, E.; Polenta, G.; Pratt, G. W.; Ramakrishnan, V.; Rastorgueva-Foi, E. A.; S Readhead, A. C.; Reinecke, M.; Remazeilles, M.; Renault, C.; Renzi, A.; Richards, J. L.; Ristorcelli, I.; Rocha, G.; Rossetti, M.; Roudier, G.; Rubiño-Martín, J. A.; Rusholme, B.; Sandri, M.; Savelainen, M.; Savini, G.; Scott, D.; Sotnikova, Y.; Stolyarov, V.; Sunyaev, R.; Sutton, D.; Suur-Uski, A.-S.; Sygnet, J.-F.; Tammi, J.; Tauber, J. A.; Terenzi, L.; Toffolatti, L.; Tomasi, M.; Tornikoski, M.; Tristram, M.; Tucci, M.; Türler, M.; Valenziano, L.; Valiviita, J.; Valtaoja, E.; Van Tent, B.; Vielva, P.; Villa, F.; Wade, L. A.; Wehrle, A. E.; Wehus, I. K.; Yvon, D.; Zacchei, A.; Zonca, A.
Publication: *Astronomy & Astrophysics, Volume 596, id.A106, 37 pp. (A&A Homepage)*
Publication Date: 12/2016
Abstract: http://adsabs.harvard.edu/abs/2016A%26A...596A.106P

Title: Are infrared dark clouds really quiescent?
Authors: Feng, S.; Beuther, H.; Zhang, Q.; Henning, Th.; Linz, H.; Ragan, S.; Smith, R.
Publication: *Astronomy & Astrophysics, Volume 592, id.A21, 29 pp. (A&A Homepage)*
Publication Date: 07/2016
Abstract: http://adsabs.harvard.edu/abs/2016arXiv160304862F

Title: Misalignment of Outflow Axes in the Proto-multiple Systems in Perseus
Authors: Lee, Katherine I.; Dunham, Michael M.; Myers, Philip C.; Arce, Héctor G.; Bourke, Tyler L.; Goodman, Alyssa A.; Jørgensen, Jes K.; Kristensen, Lars E.; Offner, Stella S. R.; Pineda, Jaime E.; Tobin, John J.; Vorobyov, Eduard I.
Publication: *The Astrophysical Journal Letters, Volume 820, Issue 1, article id. L2, 7 pp. (2016). (ApJL Homepage)*
Publication Date: 03/2016
Abstract: http://adsabs.harvard.edu/abs/2016ApJ...820L...2L

Title: What Is Controlling the Fragmentation in the Infrared Dark Cloud G14.225-0.506?: Different Levels of Fragmentation in Twin Hubs.
Authors: Busquet, Gemma; Estalella, Robert; Palau, Aina; Liu, Hauyu Baobab; Zhang, Qizhou; Girart, Josep Miquel; de Gregorio-Monsalvo, Itziar; Pillai, Thushara; Anglada, Guillem; Ho, Paul T. P.
Publication: *The Astrophysical Journal, Volume 819, Issue 2, article id. 139, 14 pp. (2016). (ApJ Homepage)*
Publication Date: 03/2016
Abstract: http://adsabs.harvard.edu/abs/2016ApJ...819..139B

Title: A young bipolar outflow from IRAS 15398-3359
Authors: Bjerkeli, P.; Jørgensen, J. K.; Brinch, C.
Publication: *Astronomy & Astrophysics, Volume 587, id.A145, 10 pp. (A&A Homepage)*
Publication Date: 03/2016
Abstract: http://adsabs.harvard.edu/abs/2016A%26A...587A.145B

Title:	Helical Magnetic Fields in the NGC 1333 IRAS 4A Protostellar Outflows
Authors:	Ching, Tao-Chung; Lai, Shih-Ping; Zhang, Qizhou; Yang, Louis; Girart, Josep M.; Rao, Ramprasad
Publication:	*The Astrophysical Journal, Volume 819, Issue 2, article id. 159, 12 pp. (2016). (ApJ Homepage)*
Publication Date:	03/2016
Abstract:	http://adsabs.harvard.edu/abs/2016arXiv160105229C

Title:	Resolved CO Gas Interior to the Dust Rings of the HD 141569 Disk
Authors:	Flaherty, Kevin M.; Hughes, A. Meredith; Andrews, Sean M.; Qi, Chunhua; Wilner, David J.; Boley, Aaron C.; White, Jacob A.; Harney, Will; Zachary, Julia
Publication:	*The Astrophysical Journal, Volume 818, Issue 1, article id. 97, 11 pp. (2016). (ApJ Homepage)*
Publication Date:	02/2016
Abstract:	http://adsabs.harvard.edu/abs/2016ApJ...818...97F

Title:	Submillimeter-HCN Diagram for Energy Diagnostics in the Centers of Galaxies
Authors:	Izumi, Takuma; Kohno, Kotaro; Aalto, Susanne; Espada, Daniel; Fathi, Kambiz; Harada, Nanase; Hatsukade, Bunyo; Hsieh, Pei-Ying; Imanishi, Masatoshi; Krips, Melanie; Martín, Sergio; Matsushita, Satoki; Meier, David S.; Nakai, Naomasa; Nakanishi, Kouichiro; Schinnerer, Eva; Sheth, Kartik; Terashima, Yuichi; Turner, Jean L.
Publication:	*The Astrophysical Journal, Volume 818, Issue 1, article id. 42, 23 pp. (2016). (ApJ Homepage)*
Publication Date:	02/2016
Abstract:	http://adsabs.harvard.edu/abs/2016ApJ...818...42I

Title:	Protostellar accretion traced with chemistry. Comparing synthetic C18O maps of embedded protostars to real observations
Authors:	Frimann, S.; Jørgensen, J. K.; Padoan, P.; Haugbølle, T.
Publication:	*Astronomy & Astrophysics, Volume 587, id.A60, 11 pp. (A&A Homepage)*
Publication Date:	02/2016
Abstract:	http://adsabs.harvard.edu/abs/2015arXiv151200416F

Title:	The Deuterium Fraction in Massive Starless Cores and Dynamical Implications
Authors:	Kong, Shuo; Tan, Jonathan C.; Caselli, Paola; Fontani, Francesco; Pillai, Thushara; Butler, Michael J.; Shimajiri, Yoshito; Nakamura, Fumitaka; Sakai, Takeshi
Publication:	*The Astrophysical Journal, Volume 821, Issue 2, article id. 94, 23 pp. (2016). (ApJ Homepage)*
Publication Date:	04/2016
Abstract:	http://adsabs.harvard.edu/abs/2016ApJ...821...94K

The Submillimeter Array (SMA) is a pioneering radio-interferometer dedicated to a broad range of astronomical studies including finding protostellar disks and outflows; evolved stars; the Galactic Center and AGN; normal and luminous galaxies; and the solar system. Located on Mauna Kea, Hawaii, the SMA is a collaboration between the Smithsonian Astrophysical Observatory and the Academia Sinica Institute of Astronomy and Astrophysics.

SUBMILLIMETER ARRAY
Harvard-Smithsonian Center
for Astrophysics
60 Garden Street, MS 78
Cambridge, MA 02138 USA
www.cfa.harvard.edu/sma/

SMA HILO OFFICE
645 North A'ohoku Place
Hilo, Hawaii 96720
Ph. 808.961.2920
Fx. 808.961.2921
sma1.sma.hawaii.edu

ACADEMIA SINICA INSTITUTE OF
ASTRONOMY & ASTROPHYSICS
P.O. Box 23-141
Taipei 10617
Taiwan R.O.C.
www.asiaa.sinica.edu.tw/